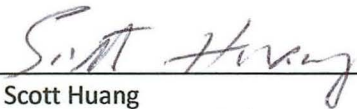



PATTERNS AND POTENTIAL SOLUTIONS TO COASTAL GEOHAZARDS AT GOLOVIN, ALASKA

By


Jacquelyn R. Smith

RECOMMENDED:


  
\_\_\_\_\_  
Dr. Scott Huang

  
\_\_\_\_\_  
Dr. Nicole Kinsman

  
\_\_\_\_\_  
Dr. Debasmita Misra,  
Advisory Committee Chair

  
\_\_\_\_\_  
Dr. Rajive Ganguli,  
Chair, Department of Mining and Geological Engineering

APPROVED:

  
\_\_\_\_\_  
Dr. Douglas Goering  
Dean, College of Engineering and Mines

  
\_\_\_\_\_  
Dr. John Eichelberger  
Dean of the Graduate School

4/22/14  
\_\_\_\_\_  
Date



PATTERNS AND POTENTIAL SOLUTIONS TO COASTAL GEOHAZARDS AT GOLOVIN, ALASKA

A

THESIS

Presented to the Faculty  
of the University of Alaska Fairbanks

in Partial Fulfillment of the Requirements

for the Degree of

MASTER OF SCIENCE

By

Jacquelyn R. Smith, B.S.

Fairbanks, Alaska

May 2014

## Abstract

The objective of this research is to measure the localized potential for shoreline change and flooding on the Golovin spit, Alaska. Long-term trends of shoreline change have been measured using multi-temporal aerial photography and satellite imagery from 1972-2013, while seasonal and annual changes in shoreline geometry have been measured by re-surveying the beach in July 2012, July 2013, and October 2013. The local bathymetry was updated with data derived from the WorldView-2 satellite to increase the spatial resolution of nearshore topography. These inputs were then integrated to establish an XBeach 1-dimensional numerical model connecting offshore storm water elevations to nearshore dynamics. The spit was found to experience episodic erosion of beach sediments, followed by sediment accretion. This resulted in a dynamic position of the shoreline, with no long-term trend in either the offshore or landward directions. Modeled storms resulted in inundation of low elevations of the spit at a 5-year return interval, with inundation of infrastructure on a 25-year return interval. The modeled results suggest overwash of the entire spit at the 50-100-year return interval. All models were based on the best available forcing data from hindcast modeling. Reinforcing and increasing the elevation of a temporary berm and/or a permanent levee structure, using a 25-year return interval as a design parameter, would help to reduce localized flooding on the spit, and may be considered in the future.



## Table of Contents

	Page
Signature Page .....	i
Title Page .....	iii
Abstract .....	v
Table of Contents .....	vii
List of Figures .....	xi
List of Tables .....	xv
Acknowledgements .....	xvii
Chapter 1 General Introduction .....	1
1.1 Storms in Northwest Alaska .....	2
1.1.1 Water Levels .....	2
1.1.2 Atmospheric Effects .....	4
1.1.3 Sea Ice .....	5
1.1.4 Sediments .....	5
1.2 Economic Impact .....	6
1.3 Evaluation of Coastal Vulnerability .....	6
1.4 Geographic Setting .....	7
1.5 Motivation and Previous Work .....	8
1.6 Research Objective .....	9

	Page
Chapter 2 Field and Remote Sensing Investigations of Barrier Spit Morphology in Golovin, Alaska.....	11
2.1 Abstract.....	11
2.2 Introduction.....	11
2.3 Study Area.....	12
2.4 Methods.....	17
2.4.1 Sediment Grain Size Measurement.....	18
2.4.2 Tides.....	19
2.4.3 Beach Profile Measurement.....	20
2.4.4 Historical Shoreline Positions.....	21
2.5 Results and Discussion.....	24
2.6 Conclusions.....	36
Chapter 3 Using WorldView-2 Multispectral Bands for Shallow Water Bathymetric Detection of Golovnin Bay and Lagoon, Alaska.....	39
3.1 Abstract.....	39
3.2 Introduction.....	39
3.3 Study Area.....	41
3.4 Methods.....	42
3.4.1 Field Measurements.....	42

	Page
3.4.2 WorldView-2 Data and Image Processing.....	42
3.4.2.1 Calibration Corrections .....	43
3.4.2.2 False Reading Removal.....	43
3.4.3 Radiance and optical reflectance relationship .....	44
3.5 Results .....	45
3.6 Discussion & Conclusion .....	50
 Chapter 4 Numerical Modeling of Coastal Morphodynamics in Response to Extreme Storm Events on the Golovin Barrier Spit in Northwest Alaska.....	
	53
4.1 Abstract .....	53
4.2 Introduction .....	54
4.3 Methods.....	55
4.3.1 Model Setup.....	55
4.3.1.1 Model Domain .....	57
4.3.1.2 Hydrodynamic Conditions .....	58
4.3.1.3 Beach Sediments .....	60
4.3.1.4 Calibration & Validation.....	60
4.3.2 Flooding Projections .....	63
4.4 Results and Discussion.....	64
4.5 Conclusions .....	78



	Page
5.0 Conclusions and Future Work .....	81
References .....	85

## List of Figures

	Page
Figure 1.1—Components of combined water level above mean sea level (MSL) during storm surge events. ....	4
Figure 1.2—Map of Golovin infrastructure and geographic location. ....	8
Figure 2.1—Regional map of study location. ....	14
Figure 2.2—Bedrock outcrops and photo samples. ....	16
Figure 2.3—Area of Interest, Golovin Spit, with labeled locations and profiles. ....	18
Figure 2.4—Example of cross-shore beach survey at inland extent of woody-wave-carried debris .....	20
Figure 2.5—Swash zone mean grain size (mm) from digital image interpretation, at profiles around the spit .....	25
Figure 2.6—Water height above sensor from July 20 to September 13, 2013, and MTL (dashed line). ....	26
Figure 2.7—Measured profiles from July 2012, July 2013, and October 2013 relative to NAVD88. .....	28
Figure 2.8—Pipe located on actively retreating bluff toe on south side of the Golovin sand spit, at Profile 1. ....	30
Figure 2.9—Intertidal scarp formed during Oct. 2013 storm at Profile 6 on end of spit (measured by Alexander Gould). ....	31
Figure 2.10— Intertidal scarp formed during Oct. 2013 storm near Profile 8, on lagoon side of spit. ....	31

	Page
Figure 2.11—Delineated shorelines of aerial and satellite imagery from 1972-2013, projected in NAD83 UTM Zone 3N on panchromatic WorldView-2 image.....	32
Figure 2.12—Net shoreline movement, projected in NAD83 UTM Zone 3N on panchromatic WorldView-2 image.....	33
Figure 2.13—Linear regression rate of change from north to south around Golovin spit, with associated 95% confidence interval at distances along the shoreline from the northern cliffs....	33
Figure 2.14—Beach width for satellite and aerial images, analyzed with DSAS. ....	35
Figure 3.1—Regional map of study area relative to the state of Alaska .....	41
Figure 3.2—Solar radiation traveling through a body of water.....	45
Figure 3.3—Exponential relationship of measured depth relative to sensor radiance for Image 1 .....	46
Figure 3.4—Exponential relationship of measured depth relative to sensor radiance for Image 2 .....	46
Figure 3.5—Classified bathymetric map of Golovnin Bay and Golovnin Lagoon.....	47
Figure 3.6—Interpolated bathymetry using WorldView-2 and surveyed data, projected in NAD83, UTM Zone 3N, datum in NAVD88.....	48
Figure 3.7—Measured vs computed depths for Image 1 .....	49
Figure 3.8—Measured vs computed depths for Image 2 .....	49
Figure 4.1—Four regimes of storm impact on the barrier environment (Sallenger, 2000) .....	55
Figure 4.2—Regional map of study location.....	56
Figure 4.3—Alongshore locations of profiles modeled .....	57
Figure 4.4—Maximum water level measured by Alexander Gould. ....	61

	Page
Figure 4.5—Measured Profile 1 before and after calibration storm event .....	62
Figure 4.6—Modeled Profile 1 before and after calibration storm event. ....	62
Figure 4.7—Maximum water elevation at the shoreline at each profile, compared to inputs.....	65
Figure 4.8—Profile 1 morphological changes with varying storm frequency .....	68
Figure 4.9—Profile 2 morphological changes with varying storm frequency .....	69
Figure 4.10—Profile 3 morphological changes with varying storm frequency .....	70
Figure 4.11—Profile 4 morphological changes with varying storm frequency .....	71
Figure 4.12—Profile 5 morphological changes with varying storm frequency .....	72
Figure 4.13—Maximum vertical translation due to erosion at each profile .....	73
Figure 4.14—Frozen slush deposited by November 2011 Bering Sea Storm.....	74
Figure 4.15—Flooding projections on the Golovin spit from numerical modeling and measured storm events.....	75
Figure 4.16—Temporary levee constructed before November 2013 storm.....	77



**List of Tables**

	Page
Table 2.1—Datasets used in DSAS .....	22
Table 2.2—Measured changes in coastal profiles annually and seasonally. ....	29
Table 2.3—Measured changes in beach width annually and seasonally.....	30
Table 2. 4—Error analysis between 1972 and 2013, with annualized error. ....	34
Table 2.5—Error due to tide at the water line. ....	36
Table 3.1—Calibration measures for Worldview2 satellite sensor .....	43
Table 4.1—Modeled storm heights at Golovin. ....	58
Table 4.2—Empirically derived wind speed and wave frequency based on mean wave height... 59	
Table 4.3—Grain size values used for model purposes. ....	60
Table 4.4—Modeled maximum water elevations and sediment redistribution at each profile ... 65	
Table 4.5—Inundation extents on the lagoon side of the spit. ....	66



## Acknowledgements

This research was funded, in part, with qualified outer continental shelf oil and gas revenues by the Coastal Impact Assistance Program, U.S. Fish and Wildlife Service, U.S. Department of the Interior. The views and conclusions contained in this thesis are those of the authors and should not be interpreted as representing the opinions or policies of the U.S. Government. Mention of trade names or commercial products does not constitute their endorsement by the U.S. Government. This research was also funded, in part, by the Alaska Space Grant Graduate Research Fellowship.

Completion of field reconnaissance was performed by authors Jacquelyn Smith and Nicole Kinsman, as well as Kimberly Tweet of the University of Alaska Fairbanks, and Alexander Gould and Meagan DeRaps of the State of Alaska Division of Geological & Geophysical Surveys. Thank you for your diligent efforts while at Golovin, and providing the comic relief necessary to roll with the punches. I would also like to thank Jack Fagerstrom for his amazing boat driving and willingness to help with tasks during my stay in Golovin.

I would like to thank my graduate committee for their guidance and support throughout my graduate program, which has extended far beyond the classroom. Particularly to Nicole Kinsman for providing a mentorship and friendship that has lead me to find a great passion for the coastal sciences and who has provided more experiences and opportunities than I could have ever asked for.

This research could not have been completed without the love and support of friends and family near and far. Thank you Levi for supporting me in all the decisions I have made and continue to make.





## **Chapter 1 General Introduction**

The 60,000 kilometers and less than 100 communities of the Alaskan coastline are subject to a wide array of coastal geohazards, some of which include storm surge induced flooding and erosion. These geohazards have become contentious social and engineering issues in the region drawing public awareness on a national scale through public media. Although many generalized reports have identified communities as being threatened by flooding and erosion (USACE, 2009; USGAO, 2003, 2009), the method of identifying these hazards at specific communities is not well established. The conflicts within the issue have led to expensive and often experimental engineering solutions, with sometimes minimal or negative effects on the hazards they are built to remediate (Mason, Jordan, Lestak, & Manley, 2012). Even though multi-temporal measurements of erosion and flooding lead to better engineering solutions, the anecdotal accounts get more public attention. This research employs community-based analysis of historical and potential geohazards for application to engineering design in Golovin, Alaska.

Golovin has been identified as one of the communities imminently threatened by flooding and erosion (USACE, 2009; USGAO, 2003, 2009). The community is currently discussing engineering solutions based on their personal experiences, and suggestions by the U.S. Army Corps of Engineers (USACE). This research uses contemporary scientific tools such as numerical modeling and remote sensing combined with field evaluations and validation to determine Golovin's vulnerability to flooding and erosion from storm surge. Measured and modeled values of flooding and erosion not only lead to better engineering designs and coastal planning, but they also legitimize community applications for federal and state funding and lead to prioritization of resource allocation for remediation projects. By using these methods, a

quantitative assessment can be made of the influence of projected and historical storm events to these particular hazards.

### 1.1 Storms in Northwest Alaska

Flooding and erosion from storms in northwest Alaska may be affected by (a) fluctuations in water elevations relative to infrastructure, (b) atmospheric influences, (c) the presence of sea ice, and (d) regular trends of sedimentation. These factors are discussed in the following sub-sections.

#### 1.1.1 Water Levels

Hazardous storm surges entering Norton Sound form in offshore low pressure systems (extratropical cyclones) and produce fluctuations in sea level at the coastline. The total water level at the shoreline has the potential to be enhanced by three factors: wind generated waves, wind generated setup, and the inverse barometric effect (Figure 1.1). When wind generated waves enter the surf zone, wave heights are enhanced (wave setup), which can be exacerbated by increased distance of open water in the direction of wind propagation, referred to as the fetch. Norton Sound is considered a shallow confined embayment at less than 20 m depth (Blier, Keefe, Shaffer, & Kim, 1997; Johnson & Kowalik, 1986; Sallenger, 1983). As extratropical cyclones move across the Bering Sea, they are constricted by Norton Sound, causing bottom shear stresses to be exerted on the column of water above, enhancing storm surge height, this is referred to as wind generated setup. The inverse barometric effect is any change in sea level due to barometric pressure differences. Water bodies will produce a “bulge” underneath a low pressure system, as water flows from high to low pressure. This sometimes initially causes set-down of water at the coastline followed by setup when the storm low reaches the shoreline.

When storm waves reach the beach, the energy of the waves are dissipated during runup (Figure 1.1). Runup can exceed the height of the combined effects of storm surge, and carry materials such as sediment and debris to its highest extent. The main components of runup includes setup, or mean shoreline position to which water begins to swash, fluctuations about that mean, and swash oscillations with periods greater than 20 seconds (Komar, 1998).

Astronomical tidal oscillations can also either enhance or diminish the effects of storm surge. Inner Norton Sound is dominated by diurnal tides (one high and one low tide per day). Mean predicted tidal fluctuations in Norton Sound range from 0.26-0.32m (NOAA, 2013). Currents induced by tides in Golovnin Bay, at Carolyn Island, are about 0.9 km/h (0.25 m/s) (Ostrom, Comiskey, & Miller, 1986), with flood tide in the north direction.

For Golovin specifically, any water pushed into Golovnin Lagoon by storm surge must also flow out post-storm. Since the Golovin spit protrudes into the lagoon entrance, a bottleneck effect is induced, forcing flood waters to inundate the northern side of the spit during ebb (Kinsman & DeRaps, 2012) (Figure 1.1). The resulting effect produces maximum flooding on the north side of the community after the maximum wind and wave conditions have passed.

When combined, these hydrologic conditions can cause extremely high water near infrastructure built on low-lying coastal features. When water reaches these normally dry elevations, this is described as inundation (NOAA, 2014b). This is the case for Golovin, which has been illustrated in Figure 1.1.

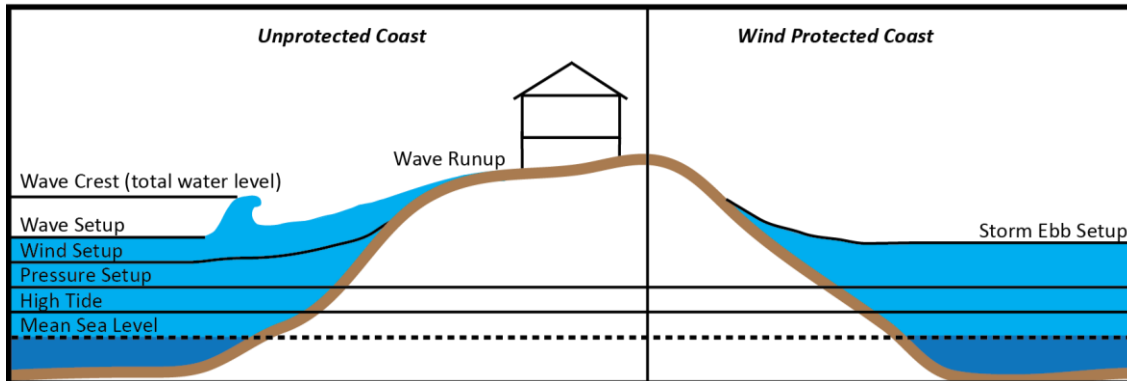


Figure 1.1—Components of combined water level above mean sea level (MSL) during storm surge events.

### 1.1.2 Atmospheric Effects

Storms typically occur during late fall and early spring. These are transitional periods between summer and winter when cold air is pushed to meet warm water which, in turn, causes air mass mixing over the Bering Sea (Ostrom et al., 1986). These air masses then travel towards Norton Sound from the southwest with prevailing wind directions.

On a global scale, ocean-atmosphere pressure oscillations are responsible for climate variations within a specified region over time. The Arctic Oscillation (AO) is a function of the polar and mid-latitude fluctuations, and is highly correlated to the North Atlantic oscillation over the northern hemisphere sub-polar region (NOAA, 2014a). These climate systems drive storminess, with low AO corresponding to wetter weather in Alaska (positive phase) (NOAA, 2014a). From the 1970's to the 1990's there was a period of positive phase AO. Since then, the AO has fluctuated both positive and negative from year to year, leading to unpredictability of the AO.

### 1.1.3 Sea Ice

When present, sea ice can protect the coastline from the effects of fall and winter storms. Ice formation on the surface of the sea reduces shear stresses produced by the wind and water interaction and shorefast ice reduces the erodibility of beach materials when waves do make it to shore. The Bering Sea currently experiences ice free conditions for approximately 5.5 months, however, increased warming in the Arctic climate which may to reduce ice extents and increase the ice free season to 8.5 months by the end of the century (Douglas, 2010). Without the protection of sea ice, coastal communities remain exposed to increased water levels and waves.

Sea Ice can also become hazardous during a storm surge. Ice has the potential to be pushed onto land by elevated water levels and onshore winds, the ice may then come into contact with infrastructure. This phenomena is called an **ice push** or **ivu**. In the November 2011 Bering Sea storm, sea ice was pushed by increased water levels and wind across the Golovin Fish camp. Fishing cabins were transported off foundations; one cabin was rafted 0.5 km by floodwaters after displacement by the ivu (Kinsman & DeRaps, 2012).

### 1.1.4 Sediments

Longshore currents in Norton Sound are dominated by northward flow along the easternmost portion of the sound and to the west on the northern portion (Sallenger, 1983). Golovnin Bay is described as a sediment sink to coarse sediments supplied by longshore drift. The sediments are derived from processes of coastal erosion on a geologic time scale (OCSEAP, 1984). The northward trend in longshore transport also persists within Golovnin Bay, made apparent by patterns of sedimentation near rivers and the bay opening. Spits protrude north and west of the linear coastline at locations of open water.

## 1.2 Economic Impact

Numerous storm surges have reached the coast of western Alaska over the past century (Wise, Comiskey, & Becker, 1981). Most events have been reported for the regional hub of Nome, although other low-lying communities are susceptible to the same storms. The documentation is limited for smaller villages with many maximum storm water elevations and estimates of resulting damages remaining unknown. The most notable event occurred in November of 1974. Damage to the city of Nome was estimated at \$12-15 million despite the addition of a protective sea wall (Blier et al., 1997). The surge height was measured at 4.0 m above mean lower-low water (MLLW), consisting of 0.2 m of tidal influence (Blier et al., 1997) and was believed to be a storm with a 50-100 year return period (Ostrom et al., 1986).

## 1.3 Evaluation of Coastal Vulnerability

The coast is a dynamic environment which exhibits changes in the nearshore due to long term morphological processes and fluctuations in water elevations. Distributions of sediments in the coastal zone are constantly responding to changing wave environments, longshore currents, and long-term sea level changes. These changes produce areas of sediment deposition (accretion), losses (erosion), or neutrality (stable). Storm surge events introduce episodic changes in morphology that may influence sediment movement despite long-term trends as well as increased elevations in water that may lead to inundation. When these processes occur adjacent to permanent infrastructure at unknown or unexpected time intervals, they become hazardous and may cause extreme fiscal and physical damages. Determining the vulnerability along a coastline to long-term processes and episodic events can lead to improved engineering and planning of the natural environment in which humans live.

In the northwest region of Alaska, coastal vulnerabilities have been identified by federal agencies in region-wide projects. The vulnerability has been assessed based on public perception which can be skewed from the morphological processes. The Alaska DGGs Coastal Hazards Program has been moving towards a systematic approach to identifying coastal hazards, focused on individual community needs. They have been collecting and analyzing science-based measurements to address the concerns of communities. Although this approach is more expensive, because of the lack of data currently available for the region, it may prove cost-saving if an engineering project is pursued for that community in the future. Information collected by this method of analysis may also help coastal managers to categorize the priority of state and federal funding of engineered projects. This science-based approach has been applied to the community of Golovin, Alaska for this research.

#### 1.4 Geographic Setting

Golovin is a blended Inupiat and Yup'ik Alaskan Eskimo village and is recognized as the Chinik Eskimo Community. The community maintains a subsistence lifestyle of fishing, hunting and gathering. There are no connecting roads between Golovin and nearby villages. Boat, air and snow machine remain the main forms of inter-village travel (Mikulski, 2009).

Golovin is located in Golovnin Bay, near northeastern Norton Sound in the Bering Sea. The Golovin spit is bordered by Golovnin Bay to the south and Golovnin lagoon to the north. The majority of the 167 people that reside in Golovin (Alaska, 2010; DCCED, 2014) reside on the spit at elevations below 10 m (relative to the North American Vertical Datum of 1988 (NAVD88)). The main infrastructure such as the school, post office, communication facilities, health clinic, fuel storage, barge landing, and commercial dock are also located on the spit (Figure 1.2). New building projects, such as residential homes, airport facilities, and other community owned



buildings have been built east of the spit at higher elevations, to reduce vulnerability to flooding. Long-term construction projects are planned for this location, however, much of the community's infrastructure remains at risk.

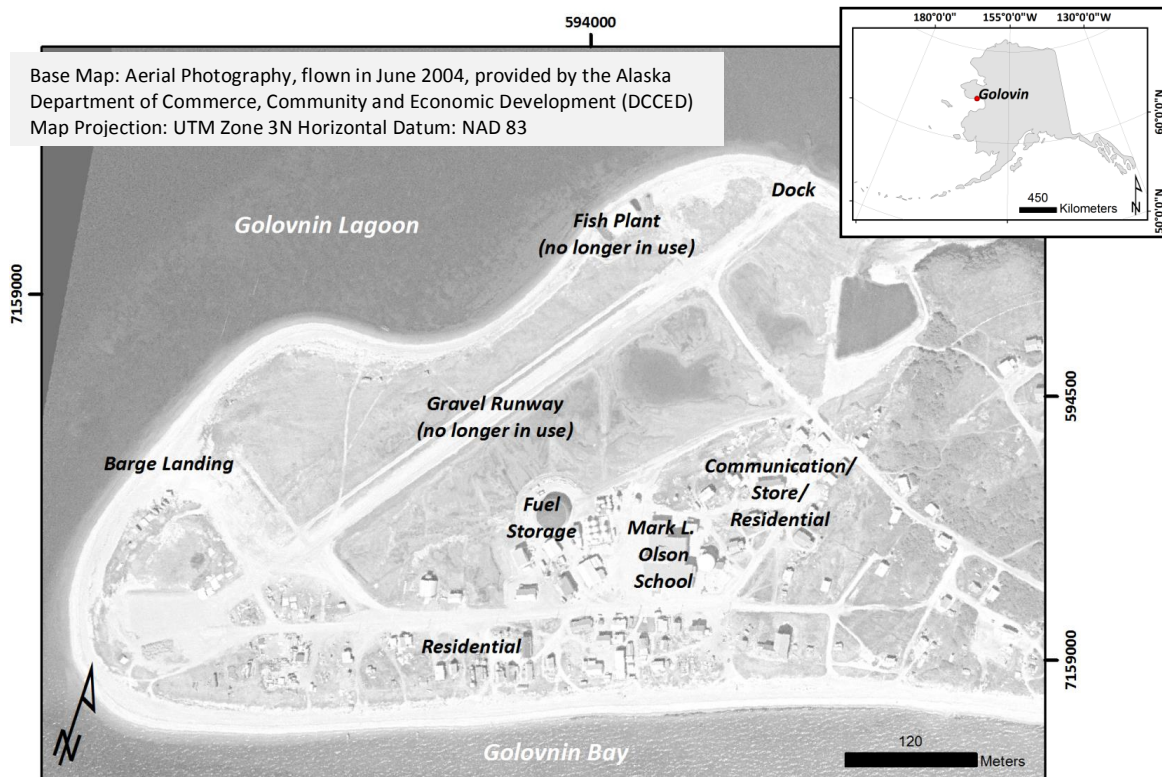


Figure 1.2—Map of Golovin infrastructure and geographic location.

### 1.5 Motivation and Previous Work

This research is being conducted on Golovin because of the frequency and magnitude of the storm events that have occurred previously, and their potential to inundate local infrastructure. Anecdotal observations have been reported by Golovin community members for flooding events in 2003, 2004 and 2005, which describe flood disasters from inundation of the main spit (Alaska, 2008, 2009). The USACE has categorized Golovin as a priority action

community for erosion problems (USACE, 2009), and has defined a flood from 1913 as the worst flooding event to have occurred (USACE, 2011a). Measurements of maximum water elevations around the Golovin spit were taken after the November 2011 Bering Sea Storm in an effort to increase baseline coastal data for northwest Alaska by the Alaska DGGs. An inundation map was published showing flooding on the main spit between 3.18 and 5.29 m relative to NAVD88 (Kinsman & DeRaps, 2012). The USACE has projected storm events with maximum surge elevations ranging from 1.83 to 4.46 m relative to MLLW (Chapman, Kim, & Mark, 2009) for return intervals of 5-100 years.

#### 1.6 Research Objective

The goal of this research is to assess the spatial vulnerability of the Golovin spit to flooding and erosion from simulated storm events and historical trends, and to provide recommendations that may contribute to future engineering design. These goals are accomplished by completing the following objectives:

1. Conduct field investigations and remote sensing analysis of historical and seasonal trends in sedimentation, including beach elevations and shoreline positions, wave and tide characteristics, and sediment sizes, types, and sources.
2. Increase spatial resolution and update nearshore bathymetry using data derived from satellite imagery and field reconnaissance.
3. Construct XBeach numerical models of projected storm surge events at profiles on the Golovin spit and correlate results with flooding around the entire spit.

This research will aid coastal managers in preparing for future events of flooding and erosion. An updated map of potential flooding corresponding to storm water elevation predictions will provide the residents of Golovin with information needed to prepare for a storm

event, which may lead to decisions on whether to stay and bolster community infrastructure, or to migrate for concerns of safety. Because of the lack of oceanographic sensors and up-to-date modeling, these decisions are currently not clear for coastal managers within communities, but this research may contribute to the decision making process. The flooding map will also provide potential inundation heights useful for engineered design of remediation structures.

Many communities in northwest Alaska experience similar geohazards with the same anecdotal explanation of storm histories. These communities may benefit from a similar approach to identifying and projecting coastal vulnerability for future planning.

## **Chapter 2 Field and Remote Sensing Investigations of Barrier Spit Morphology in Golovin, Alaska**

### **2.1 Abstract**

Field investigations of the Golovin, Alaska spit were conducted in July 2012, July 2013, and October 2013. In this research, data collected during field reconnaissance were combined with interpretations of satellite and aerial imagery for the investigation of the coastal morphodynamics of the spit where a portion of the community of Golovin is located. Investigation revealed that long-term and yearly measurements of shoreline positions showed minimal trends of shoreline change, with some specific locations experiencing larger fluctuations in seaward and landward movement of the shoreline. The more dynamic shoreline positions were located on the tip of the spit, with less dynamic shorelines on the bay and lagoon side of the spit, resulting in different long-term shoreline envelopes. The seasonal shoreline envelopes reflected the same trends, with beach volume and width envelopes increasing at the tip of the spit. Beach material was dominated by very fine gravel that was fine skewed, very platykurtic, and moderately sorted, which may indicate sedimentation dominated by the proximity to sediment supply rather than hydraulic forcing. The proximity of the sediment supplying the beach and the spatial distribution of all shoreline envelopes makes Golovin less subject to long-term erosion rates than was previously expected. Golovin, however, may have experienced episodic erosion of sediments that were replenished over time.

### **2.2 Introduction**

The dynamic nature of the coastal environment leads to seasonal and annual variation in beach morphology. A stable shoreline generally remains within a range of typical volumes and widths on a yearly basis (an envelope), with changes occurring from summer (normal) to winter

(storm/swell) due to variable wave energy (Komar, 1998). Departures from this envelope are considered erosion or accretion. Grain size distributions along the shoreline and across the shoreface are representative of the depositional environment (Komar, 1998). When beaches are abutted by human infrastructure, the infrastructure is also subject to the dynamic nature of coastal processes, which can lead to coastal vulnerability.

In northwest Alaska, communities built on low-elevation coastal plains are particularly vulnerable to flooding and erosion from extratropical cyclones during fall storm seasons (Alaska, 2008, 2009; Chapman et al., 2009; Kinsman & DeRaps, 2012; USACE, 2009; USGAO, 2003, 2009; Wise et al., 1981). Sea ice extents in the Bering Sea have been projected to decline through the next century, with increases in the ice-free season from 5.5 months to 8.5 months (Douglas, 2010). For the entrance of Golovnin Bay, freeze-up and break-up have remained relatively consistent from 1853 to 2013 (ACCAP & SNAP, 2014), but historical sea ice cover within the bay is unknown. Reductions in sea ice have the potential to leave the coastline exposed during the regular storm seasons. Although these events are known to occur, there is limited baseline data available for most communities in the region, and associated rates of erosion and locations of inundation extents remain predominately anecdotal.

### 2.3 Study Area

The barrier spit of Golovin, Alaska is home to 167 people, including members of the Chinik Eskimo community (DCCED, 2014). The people of Golovin use the beach for summer and winter subsistence activities, such as fishing and hunting. The beach is also a location of travel by all-terrain-vehicle, which is common for most community members. The beach adjacent to the Cheenik River has been mined for road surface materials, but the rates and frequency of beach mining are unknown.

The Golovin spit is located along the northeastern coastline of Norton Sound, within the Bering Sea. The spit protrudes into the neck between Golovnin Bay to the south, and Golovnin Lagoon to the north (Figure 2.1). The Yuonglik River delta empties into Golovnin Lagoon from the north. The surrounding coast of the lagoon consists of a combination of exposed bedrock shoreline, tundra, and vegetated overwash deposits. Sediment deposition by river outlets shows longshore current transport of sediments to the north and west along the coastline within Golovnin Bay. Longshore currents within Golovnin Lagoon, however, show no significant trend. The tidal energy at Golovin is mesotidal and diurnal.

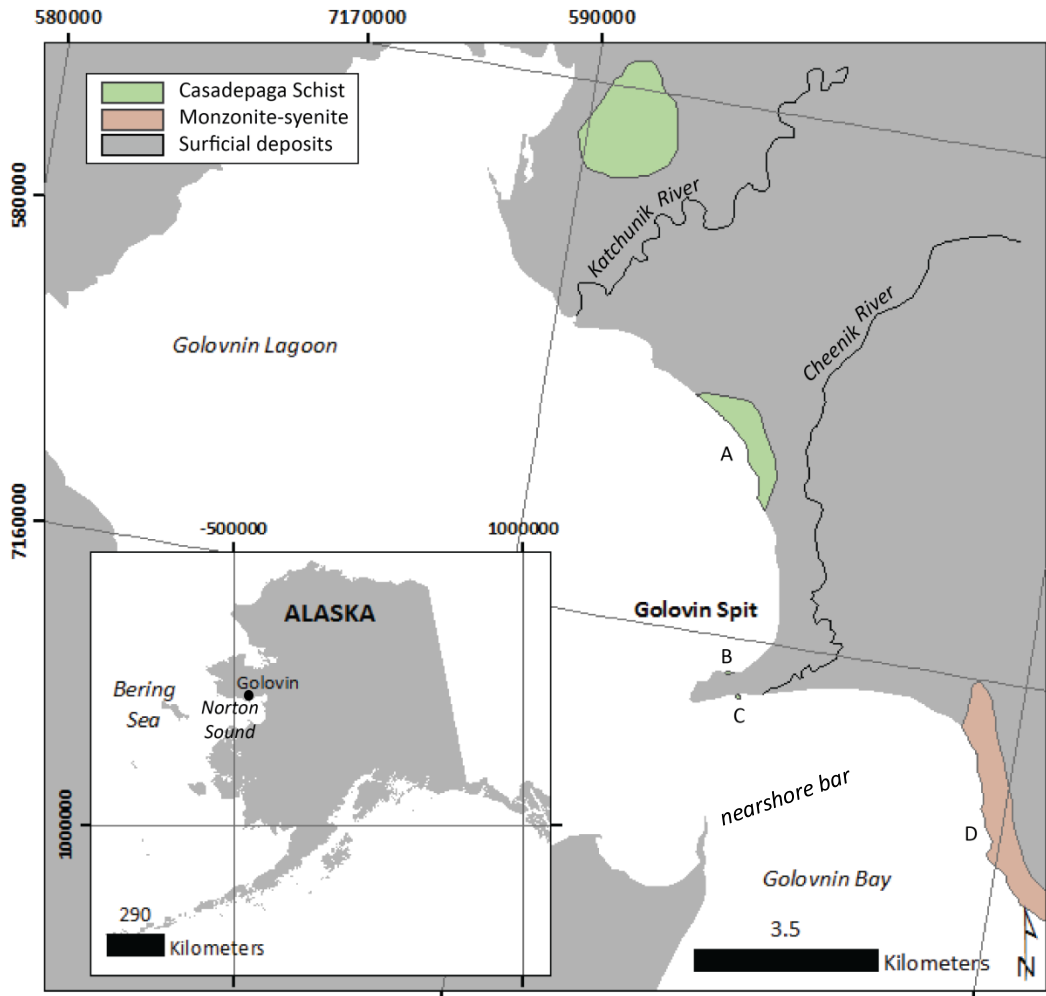


Figure 2.1—Regional map of study location. Profiles represent measured locations approximately 500 m alongshore around spit, bedrock locations are labeled and shown in Figure 2.2 (bedrock interpreted from geologic map (Till, Dumoulin, Werdon, & Bleick, 2010), field reconnaissance). Zoomed-in data is projected in NAD83 UTM Zone 3N, zoomed-out data is projected in NAD83 Alaska Albers.

A nearshore bar system is present offshore of the bay side of Golovnin which is unique (Figure 2.1). There is a spit located on the opposing shoreline, although much smaller, the spit

extends beyond the shoreline, reducing the water depths to a few meters as much as 3 km into the bay. This bar system protects the Golovin coast from potential wave attack induced by the large fetch extending into Norton Sound. There is also a channel between the bar system and the Golovin coast. The channel reaches depths of about 10 m, which dissipates hydraulic energy as breaking waves enter.

There are two prominent bedrock deposits present along the Golovin coast, as shown in Figure 2.1 and 2.2. One is the Casadepage Schist, to the north (Figure 2.2A-C), which consists mainly of dark-green, chlorite-rich schist with plagioclase, chlorite, white mica, and quartz (Till et al., 2010). The plutonic igneous rock, to the south (Figure 2.2D), is a monzonite-syenite consisting mostly of plagioclase and alkali feldspar (Till et al., 2010).

No permanent tide gauge or water level indicator is present near Golovin. The closest tide gauge is located in Nome, Alaska, approximately 170 kilometers along the coastline. The tide measured at Nome is translated to tidal predictions modeled at Carolyn Island, in Golovnin Bay. The community regularly experiences elevated water levels due to storm events, which have flooded community infrastructure, however, there are minimal measurements of these events, because of the lack of a permanent water elevation monitoring station or GPS surveying.





Figure 2.2—Bedrock outcrops and photo samples: (A)-(C) Schists and (D) monzonite-syenite, letters correspond to locations in Figure 2.1.

## 2.4 Methods

Long-term and seasonal beach morphology supports the assessment of coastal vulnerability of infrastructure by providing expected values of regular changes in the dynamic beach environment. Surveys of beach elevation profiles, sediment characterizations, and hydraulic fluctuations/datums were carried out in July 2012, July 2013, and October 2013 to contribute to measurements of beach volumes, widths, grain size distribution and source descriptions, and tidal amplitudes and phases. Nine transects were measured around the Golovin spit at distances of 250 m alongshore (Figure 2.3). A combination of sediment samples were collected physically and with digital images at the vegetation line, locations of surface grain size transitions, mid-beach, and in the swash zone at each of the profiles. A pressure transducer was deployed on the lagoon side of the spit to measure water levels over a three month period. Since historical beach profiles were not measured, 5 aerial and satellite images of the study location acquired from 1972 to 2013 were used to interpret the horizontal position of the shoreline over time.

To aid the analysis of this research, the following measurements were made as described in more detail in the following sub-sections:

- Sediment grain size distributions.
- Tidal datum and fluctuations.
- Beach profile measurements.
- Historical shoreline positions.



Figure 2.3—Area of Interest, Golovin Spit, with labeled locations and profiles, projected in NAD83 UTM Zone 3N on panchromatic WorldView-2 image.

#### 2.4.1 Sediment Grain Size Measurement

This research has incorporated an automated grain size measurement algorithm for digital image interpretation of grain size distribution developed by the U.S. Geological Survey Pacific Coastal and Marine Science Center (Warrick et al., 2009). The image autocorrelation algorithm was used to detect a pixel to length correlation factor for each digital image which was then applied to identify and measure individual grain sizes. Using this technique the grain size was calculated based on a two-dimensional form in the frequency domain, eliminating the need for physical samples in the calibration process (Buscombe, Rubin, & Warrick, 2010).

For this research, both physical and image-based samples were taken in the field to determine the standard error between the digital image and sieved samples. Nine physical

samples were collected across and alongshore around the Golovin spit and were sieved to determine the cumulative grain size distribution. A linear relationship between sieved sediment sizes was assumed to determine the exact value of percent passing for  $D_5$ ,  $D_{10}$ ,  $D_{16}$ ,  $D_{25}$ ,  $D_{50}$ ,  $D_{75}$ ,  $D_{86}$ ,  $D_{90}$ , and  $D_{95}$  and to allow for direct comparison between the sieved and image-based results.

#### 2.4.2 Tides

A *Solinst Levellogger* pressure transducer was deployed at a location protected from wave activity on the northeast side of the spit from July to October 2012. The water level data was collected in units of pressure (kPa) every ten minutes. From the pressure data, a correction was made based on atmospheric pressure conditions recorded at the local airport (approximately 7.2 m above MTL) (ISUST, 2013). The atmospheric pressure was subtracted from the pressure reading of the transducer. A conversion factor was then applied to convert the pressure to water column height, with an assumed seawater density of  $1025 \text{ kg/m}^3$ , which is common for saline seawater. A water height measurement was taken during installation and used to calibrate the measurements converted from the pressure transducer. The difference between the measured and derived height was 0.0688 m, this value was added as an adjustment to the entire dataset.

To calculate the local tidal datum and range, the corrected water level time series was input into the `t_tides` Matlab script (Pawlowicz, Beardsley, & Lentz, 2002). The script was developed to interpret tidal constituents using harmonic analysis, which modeled the data as a sum of sinusoids at frequencies relative to astronomical parameters (Pawlowicz et al., 2002). The major tidal constituents at similar frequencies were summed to produce the tidal range. The MTL was directly calculated by the `t_tides` script at 1.28 m above NAVD88.

### 2.4.3 Beach Profile Measurement

Beach profiles were measured perpendicular to the coastline around the barrier spit during each of the field excursions (Figure 2.4). A GPS base station (TopCon HiPerII) was placed on USLM monument 3651 at the top of the cliffs overlooking Golovin to provide real-time-kinematic corrections to a rover GPS. Each profile included specified locations of significant across-shore features, such as dune fields, vegetated zones, high water lines, wrack, changes in grain size, and breaks in slope. All of the measured elevations have been post-processed with the [Top Con] Tools software and are presented relative to NAVD88. Vertical precision of the survey ranged from 0.40-0.65 cm, with 1.10-0.11 cm horizontal precision.



Figure 2.4—Example of cross-shore beach survey at inland extent of woody-wave-carried debris (Kimber Tweet holding the GPS rod).

Relative beach volume was computed in Matlab as the area under the measured profile within the spatial bounds shared by the profiles. Beach slopes were measured by taking the average slope between points measured along each profile between the vegetation line and swash zone. The beach width, in this study, is defined as the horizontal distance between the vegetation line and that of the mean tide level (MTL) at each profile.

#### 2.4.4 Historical Shoreline Positions

Historical rates of shoreline change were analyzed using the Digital Shoreline Analysis System (DSAS) toolbox incorporated into Environmental Systems Research Institute (ESRI) Geographic Information System (ArcGIS) (Thieler, Himmelstoss, Zichichi, & Erugl, 2009). Vegetation lines on five aerial and satellite images (see Table 2.1) were hand digitized as polyline feature classes. Transects were cast, from an offshore baseline, perpendicular to the shorelines at 50 m intervals alongshore. A least-squares regression was performed on shoreline positions representing time periods between 1972 and 2013 for each transect. The weighted linear regression rate-of-change was then derived from the annualized rate of change of the least-squares regression, weighted by the error associated with each photo, using the calculate statistics tool of DSAS.

The vegetation line was chosen as a shoreline proxy rather than the mean high water line (MHWL) for this study because of the unavailability of tidal data and the resolution of the imagery. Since no permanent tide gauge was present near Golovin, tidal corrections could not be applied. Also, the spatial resolution of the aerial and satellite imagery was not high enough in all cases to resolve the location of the MHWL. The vegetation line, however, was visible in all images. The instantaneous water line and the vegetation line were used to measure beach width. Although errors were increased because of the lack of tidal data, the errors were

accounted for by determining the range of horizontal change in water level over the slope of the beach at each profile, which is reduced with increased steepness of the beach (Moore, Ruggiero, & List, 2006; Robertson, Whitman, Zhang, & Leatherman, 2004).

Table 2.1—Datasets used in DSAS

Image Source	Type	Acquisition Date	Pixel Size	Number of GCP's	Geo-model RMS Error
USGS <sup>1</sup>	Aerial Photography	8/1/1972	4.50 m	7	1.31
AHAP <sup>2</sup>	Aerial Photography	7/1/1980	1.66 m	11	0.58
DCCED <sup>3</sup>	Aerial Photography	6/11/2004	0.61 m	-	0.61
SPOT5 <sup>4</sup>	Multispectral Satellite Imagery	9/9/2009	2.50 m	11	0.88
Worldview-2	Panchromatic Satellite Imagery	9/17/2013	0.50 m	11	0.30

<sup>1</sup>U.S. Geological Survey, <sup>2</sup>Alaska High Altitude Photography, <sup>3</sup>Alaska Department of Commerce, Community and Economic, Development (DCCED), <sup>4</sup>*Satellite Pour l'Observation de la Terre 5*

The 2004 aerial image was an orthorectified product made available by the Alaska DCCED and was rectified to a precision of 90% of the points within 0.61 m. All other datasets were georeferenced, image to image, with the 2004 image in the Excelis VIS ENVI software map rectification module. The datasets were cropped to an area of interest, focused on the Golovin spit. It was not critical to orthorectify all of the datasets because of the small study area and minimal changes in elevations within the study area. Each of the datasets were georeferenced using either the 1<sup>st</sup> order (for 1972) or the 2<sup>nd</sup> order (all other) polynomial geometric models with 7-11 ground control points.

Inherent errors were introduced during georeferencing of the imagery and geolocation of the shoreline. For non-orthorectified products, Del Rio and Garcia (2014) apply the following

equation to access the total error in the position of the shoreline from an aerial image, the equation has been modified to reflect the errors in this analysis:

$$E_p = \sqrt{G^2 + R^2 + C^2} \quad (2.1)$$

Where  $G$  is the error due to georectification,  $R$  is the error due to the spatial resolution of the image, and  $C$  is the error due to large changes in elevation. The georectification error was calculated by adding the sum of the squares for the error produced by georeferencing the images to the 2004 orthorectified image and the error of the orthorectified product. The error due to differing ground resolution was calculated as the sum of squares of the ground pixel size of the image and the error due to digitizing. The digitizing error was calculated by a single operator digitizing the same feature three times and calculating the average distance between the features. The error due to changes in elevation was assumed to be zero, because of the small changes in elevation at the vegetation line and lack of cliffed features.

The annualized error was determined using Equation 2.2 (Del Rio & Garcia, 2014).

$$E_{RATE} = \frac{\sqrt{E_{p1}^2 + E_{p2}^2 + E_{p3}^2 + E_{p4}^2 + E_{p5}^2}}{T} \quad (2.2)$$

Where the sum of the squares of error from each of the images was divided by the total timespan of the images (in years). For beach width calculations, error was enhanced at the water line by variations in water elevations relative to the MTL. The error was calculated as the horizontal distance the tidal range would have covered relative to the slope of each profile measured in 2012. This measure of error did not include runup, swash, setup, or a tidal datum (for digital elevation models), which increased horizontal positioning errors (Moore et al., 2006; Robertson et al., 2004). Since the images were taken during summer and early fall, changes in the water line and beach widths may have occurred due to seasonal changes. This added error



to the analysis as well, when comparing the beach widths directly from one time period to the next. Instead, discussion on this topic will remain within a broad realm, addressing only relative trends.

## 2.5 Results and Discussion

The Golovin gravel spit is composed of very fine sand to medium gravel, with a mean grain size of 2.72 mm +/- 0.68 mm. The grain size distributions are fine skewed, very platykurtic with moderate sorting. The majority of beach material is composed of monzonite-syenite weathered product, with large platy schist gravel on the surface. The mean grain size decreased in the swash zone with distance from the sediment source, until about 300 m from the end of the gravel spit, with a slight increase in mean grain size down-shore from the river outlet. The beach material then increased in grain size beyond the very northern portion of the sand spit.

The composition of nearshore sediments suggests transport by longshore currents from in-situ monzonite-syenite bedrock approximately 6 kilometers southeast along the coast as well as from suspended sediment in the Cheenik River. The reduction in grain size along the coastline implies grain size selective rates of longshore transport during littoral drift. The slight increase in grain size and increase in beach width after the river outlet suggests either the addition of material from erosion of the backshore, or sediment input from the Cheenik River. The grain size increased again near the end of the spit corresponding to an increase in wave energy near the channel into Golovnin Lagoon. The increase in grain size on the northern portion of the spit is likely due to the reverse transport of sediments from the adjacent Schist cliffs extending along 5 kilometers of coastline directly north.

The grain size distributions around the Golovin spit were atypical of common beach sediments. Most coastal grain size distributions are highly-sorted, fine-grained and leptokurtic.

The sediments around the Golovin spit however, were only moderately sorted, coarser-grained, and very platykurtic. This suggests a lack of hydraulic forcing on most portions of the beach face, which could be due to low energy tidal and wave environments, the presence of landfast sea ice during large portions of the year, and close proximity to sediment sources. It is likely that all of these explanations are applicable in Golovin, because of the minimal tidal range (0.43 m; discussed later in this section), the protection of the spit from offshore waves by the presence of a complex nearshore bar system, susceptibility to sea ice during the winter months, and apparent sediment sources adjacent to the spit. The sediments were defined as fine-skewed, which is expected for all coastal sediments, as the fine-grained material is unable to break suspension until very low current velocities are experienced.

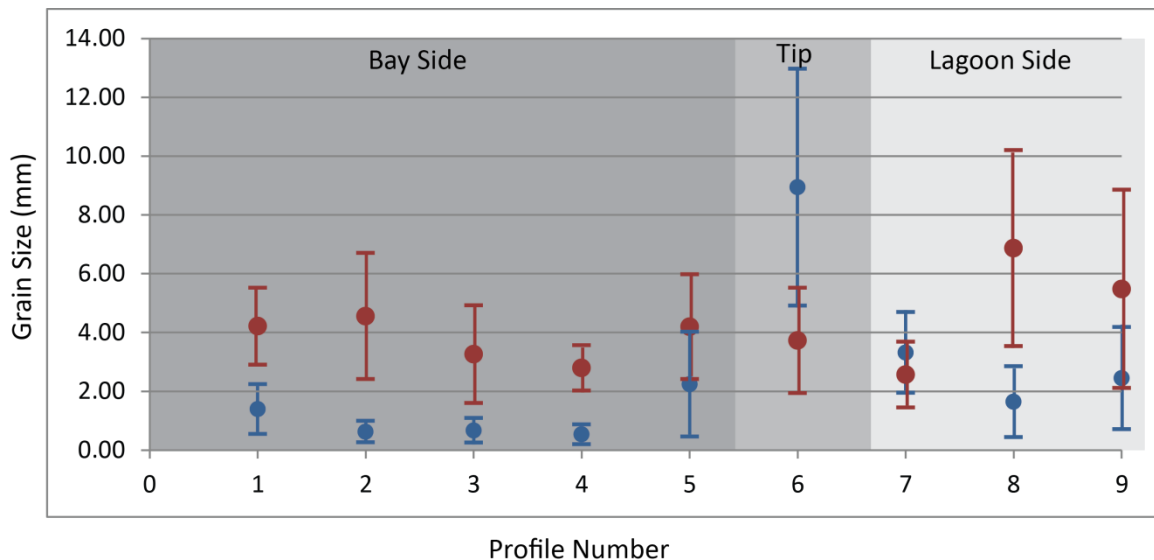


Figure 2.5—Swash zone mean grain size (mm) from digital image interpretation, at profiles around the spit for July 2012 (blue) and July 2013 (red).

From July 2012 to July 2013, mean grain size in the swash zone increased by two to five mm (Figure 2.5). This change occurred at all locations around the spit, except for at the tip, which decreased in grain size. This may have been the result of a slight increase in wave energy, or a combination of added sediment from a nearby source and changes in wave energy. Beach width was increased at most locations on the front of the spit during the same time period, which would occur from a changing wave environment, or the erosion of the vegetation line, which occurred at Profile 1.

The mesotidal conditions at Golovin resulted in a diurnal tidal range of 0.43 m, with an approximate tidal volume of  $5.9 \times 10^7 \text{ m}^3$ , for the  $137.2 \text{ km}^2$  tidal prism of Golovnin lagoon. The mean tide level was identified as 1.51 m above the sensor (Figure 2.6), which corresponds to +1.28 m relative to NAVD88.

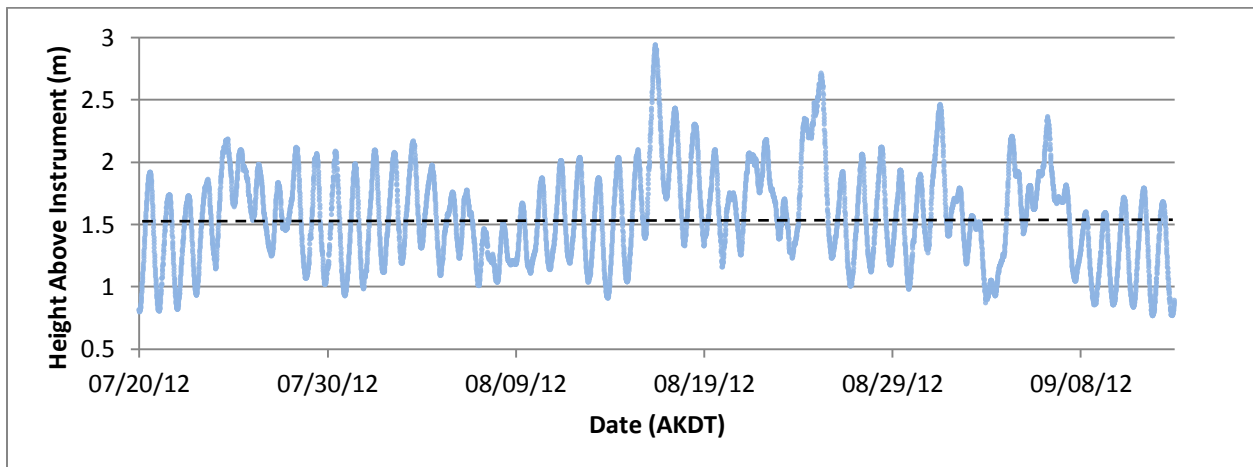


Figure 2.6–Water height above sensor from July 20 to September 13, 2013, and MTL (dashed line).

Although regular tidal energy was considered low, the water elevations induced by storm surge may have an effect on transport of sediment above the high water line (HWL). The

U.S. Army Corps of Engineers (USACE) reported storm elevation return intervals between five and 100 years of 1.83-4.46 m relative to MLLW (Chapman et al., 2009). These storm elevations are non-inclusive of runup, which would increase the maximum water elevations reached on the beach. The offshore modeled wave heights have been reported as a frequency-of-occurrence relationship as well, as a part of the wave information studies completed by the USACE. The values for maximum mean offshore wave height correspond to 3.0-5.7 m in height for return intervals of one to 100 years (USACE, 2013). Once propagated onshore, these values would be decreased tremendously because of the complex offshore bar system protecting the Golovin spit. The vegetation elevations around the spit were four to five meters relative to NAVD88 for the front and two to three meters relative to NAVD88 for the back and tip of the spit. The modeled storm elevations not only have the potential to inundate higher than the vegetation line, but may do so at a high frequency (at least every five years) on the back of the spit (see Figure 2.7).

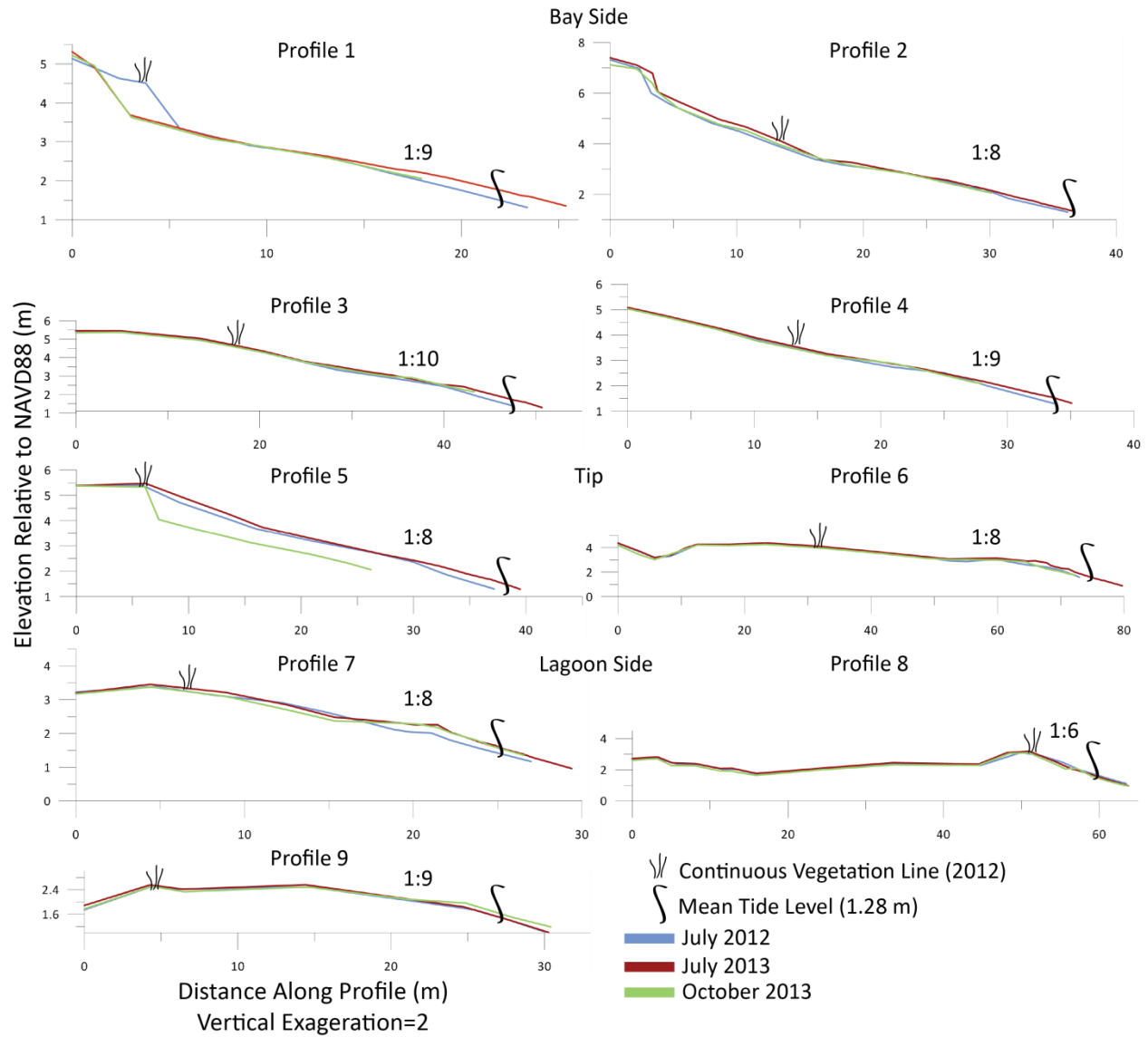


Figure 2.7—Measured profiles from July 2012, July 2013, and October 2013 relative to NAVD88.

Beach profile measurements taken during the three field seasons are shown in Figure 2.7. Changes to the beach volume and slope annually and seasonally are reported in Table 2.2. Measured changes in beach slope were minimal compared to the overall beach slope. Beach volume was consistently reduced from the summer to the winter profile except for Profile 2, in

which beach volume increased. Profile 1 decreased in volume from 2012 to 2013, with an associated increase in beach width. An apparent erosional feature was also observed at the vegetation line (Figure 2.8) of Profile 1. An abandoned municipal water supply pipe was transported from the bluff crest to the beach surface from 2012 to 2013. Some locations near measured profiles experienced removal of sediment during the beginning of the winter storm season (Figures 2.9 & 2.10). The sediment was removed below the vegetation line, resulting in escarpment, or seasonal erosion. This also resulted in a decrease of beach volume from summer to winter, resulting in seasonal beach volume envelopes on average of 0.4 m<sup>3</sup> for the bay side, 14.3 m<sup>3</sup> for the tip, and 3.0 m<sup>3</sup> for the lagoon side.

Table 2.2—Measured changes in coastal profiles annually and seasonally.

Profile	Average Summer Slope (m/m)	Annual Change in Slope (%) (2012-2013)	Annual Change in Volume m <sup>3</sup> (2012-2013)	Seasonal Change in Volume m <sup>3</sup> (Summer to Fall)	Change in Volume m <sup>3</sup> total
1	0.110	-11.3	-1.63	-0.77	-2.41
2	0.133	-13.2	4.7	3.79	0.91
3	0.105	-7.4	4.46	-2.95	1.51
4	0.115	-9.0	1.46	-1.67	-0.21
5	0.120	-12.8	3.08	-18.96	-15.88
6	0.120	42.9	7.29	-9.63	-2.33
7	0.130	26.2	2.24	-1.76	0.47
8	0.160	15.1	3.12	-7.07	-3.94
9	0.110	-2.4	1.65	-0.19	1.45

The beach width increased from 2012 to 2013 for all of the profiles except Profile 5 (Table 2.3). Minimal changes in beach width occurred from summer to winter, except for Profiles 5 and 6, which had increased beach widths. The seasonal envelope for beach width was 0.3 m on the bay side, 7.1 m on the tip, and 0.1 m on the lagoon side.

Table 2.3—Measured changes in beach width annually and seasonally.

Profile	July 2012 Beach Width (m)	July 2013 Beach Width (m)	October 2013 Beach Width (m)	Annual Change in Beach Width (2012-2013) (m)	Seasonal Change in Beach Width (Summer to Fall) (m)
1	19.90	24.83	24.45	4.94	-0.38
2	23.58	23.70	24.05	0.12	0.35
3	23.14	25.92	26.95	2.78	1.03
4	23.23	25.09	29.89	1.86	4.80
5	21.33	19.70	29.00	-1.63	9.30
6	42.64	45.45	45.22	2.81	-0.24
7	13.95	14.62	14.49	0.67	-0.13
8	7.03	7.30	6.83	0.27	-0.47
9	24.16	24.27	25.32	0.11	1.06



Figure 2.8—Pipe located on actively retreating bluff toe on south side of the Golovin sand spit, at Profile 1.



Figure 2.9—Intertidal scarp formed during Oct. 2013 storm at Profile 6 on end of spit (measured by Alexander Gould).



Figure 2.10— Intertidal scarp formed during Oct. 2013 storm near Profile 8, on lagoon side of spit.

The reductions in beach volume from the summer to the winter beach profiles, is typical of seasonal changes in beaches globally. As wave energy increases in the winter, sediment is removed from the beach face and stored in offshore bars, only to return when the wave energy is reduced again. These changes were more significant, resulting in a larger envelope for both beach width and volume, on the tip of the spit than on either the lagoon or bay side. Profile 5



experienced a large seasonal change in beach width and volume, and was the only profile on the south side of Golovin to experience a large seasonal loss. The changes to Profile 1 from 2012 to 2013 were substantiated through the winter profile, suggesting permanent erosion of the coastal bluff. All other profiles showed minimal increases in beach area annually.

Long-term shoreline trends were both seaward and landward on an inter-annual timescale, with the most seaward shoreline position in 2013 for most locations around the spit (Figure 2.11). The long-term envelope of shoreline movement, which represents the distance between the two farthest shoreline proxies, is shown in Figure 2.12. The non-linear shoreline movement was within a minimal range on the bay side of the spit compared to the lagoon side, which exhibited a maximum range of movement at the lobes and tip of the spit. The weighted linear regression rates-of-change reflected similar trends. The rates were minimal and ranged from positive to negative within the bounds of error (confidence interval of 95%) (Figure 2.13).



Figure 2.11—Delineated shorelines of aerial and satellite imagery from 1972-2013, projected in NAD83 UTM Zone 3N on panchromatic WorldView-2 image.



Figure 2.12—Net shoreline movement, projected in NAD83 UTM Zone 3N on panchromatic WorldView-2 image.

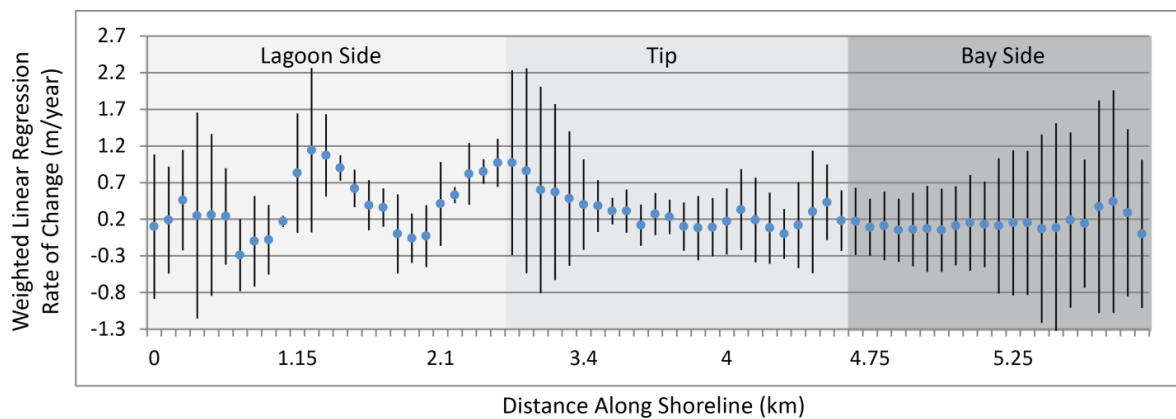


Figure 2.13—Linear regression rate of change from north to south around Golovin spit, with associated 95% confidence interval at distances along the shoreline from the northern cliffs.

The non-linear rates-of-shoreline change increased linear-regression errors for the entire spit (Figure 2.13). Annualized error at the vegetation line from the entire dataset was

found to be 0.19 m/year, which was similar to many of the rates found for shoreline change (Table 2.4). The non-linearity of the shoreline change shows the highly dynamic nature of the physical processes on the Golovin spit. Locations that were highly dynamic were the tip of the spit, and one lobe on the lagoon side, which corresponded to the results from the GPS survey (since the lobe was not surveyed). These locations accrete sediment, which may be eroded periodically, with no significant net change in shoreline position. The bay side of the beach was much less dynamic, with smaller long-term shoreline envelopes. Erosion did occur on the less dynamic portion of the beach (bay side) at Profile 1. These results may be representative of a single erosion event that was captured during 2012 and 2013, which may return to a less dynamic shoreline in the long-term.

Table 2. 4—Error analysis between 1972 and 2013, with annualized error.

Dates	Time Period (years)	Total Error (m)	Annualized Error (m/year)
1972	-	5.30	-
1980	8	3.03	0.76
2004	24	2.61	0.17
2009	5	3.62	0.89
2013	4	2.53	1.10
1972-2013	41	-	0.19

\*The annualized error is calculated between the each adjacent time period

Most of the long-term time periods showed an expected trend of wider beach widths near the river outlet to the west (Figure 2.14). A notable exception was the 1972 shoreline, which had lower beach width at that location. Large increases in beach width occurred in 1980 and 2009. Beach width was consistently smaller on the back side of the spit, with the most extreme lows in 2013. The end of the spit had similar beach widths to the front of the spit, with a few large transects on the very end.

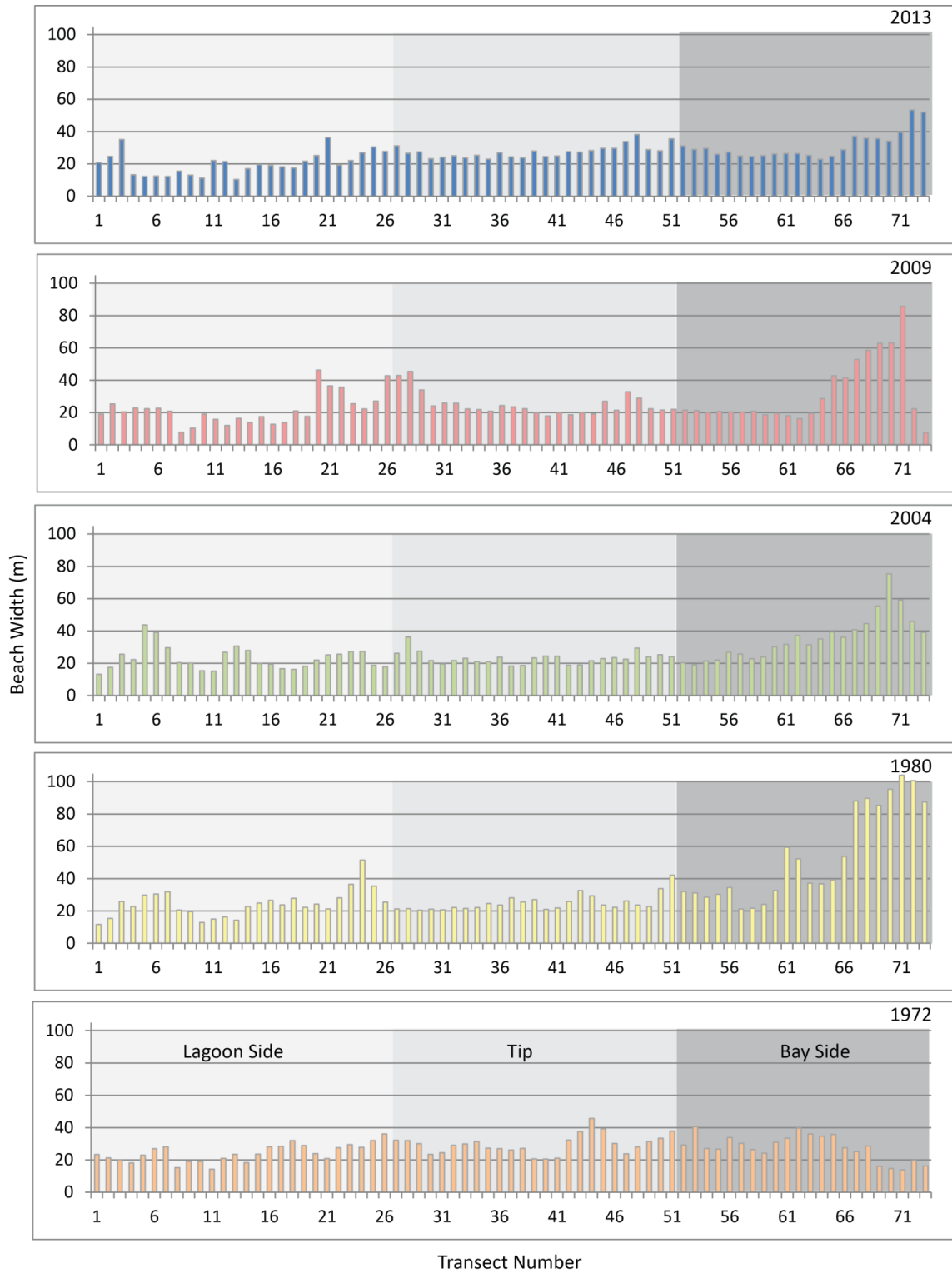


Figure 2.14—Beach width for satellite and aerial images, analyzed with DSAS.

Wider beach widths near the Cheenik River coincided with widened beaches near the end of the spit in the 1980 and 2009 images. Since this is a location of episodic beach mining, and, by definition, longshore transport is known to travel through this point, the beach width along the entire spit may be subject to changes due to the propagation sediment losses. There are no records for the volume of beach sediments mined from this region, so a quantitative relationship cannot be acquired. However, if beach widths near the Cheenik River are impacted by mining activity, mining may also affect beach width at the tip of the spit.

The possible error in beach width due to water level fluctuations was on average 3.56 m (Table 2.5) for all profiles. This value is large in comparison to the smaller beach widths, but insignificant for very large beach widths, although this value of error does not incorporate all potential errors.

Table 2.5—Error due to tide at the water line.

Profile	Slope (m/m) July 2013	Tidal Range (m)	Water Level Error (m)
1	0.110	0.43	3.91
2	0.133	0.43	3.23
3	0.105	0.43	4.10
4	0.115	0.43	3.74
5	0.120	0.43	3.58
6	0.120	0.43	3.58
7	0.130	0.43	3.30
8	0.160	0.43	2.69
9	0.110	0.43	3.91
		<b>Average</b>	<b>3.56</b>

## 2.6 Conclusions

The long-term sedimentary environment of the Golovin spit is likely dominated by sediment inflows from nearby sources rather than wave or tidal energy. The sediment inflows

provide an excess of material to the spit, which is eroded periodically, resulting in dynamically stable shoreline positions. Beach mining near the mouth of the Cheenik River may also affect sedimentary trends, reducing the amount of sediment supplied by longshore transport.

The Golovin spit is subject to storm surges that increase water levels to conditions inducing sediment transport at locations around the spit, but these events do not appear to induce long-term trends of erosion. They may, however, be responsible for the seasonal variability in shoreline change and beach width. These increased water elevations do have the potential to reach community infrastructure. The back of the spit exhibits a lower threshold for storm flooding based on the lower coastal elevations measured at the vegetation line, and may flood on a more regular basis than from the bay side of the spit.

Despite common perception, the results of this analysis did not produce large trends of erosion at any point on the spit. This research provides quantitative measurements that can be applied to coastal decision making and engineering. Analyses of this nature may be important for engineering decision making throughout all of northwest Alaska, in communities that experience similar geohazards. For the community of Golovin in particular, this may reduce the economic impact of engineering design to remediate coastal hazards, because erosion is not a key issue. The data collected in this research may be used as a baseline for future measurements of changes in Golovin beach morphology, particularly after large storm events to expand the understanding of coastal morphology in the region.



## **Chapter 3 Using WorldView-2 Multispectral Bands for Shallow Water Bathymetric Detection of Golovnin Bay and Lagoon, Alaska**

### 3.1 Abstract

Storm surge flooding and erosion may be best quantified with robust hydrodynamic computer models of potential storm events. These computer models require high resolution bathymetric data, which is currently unavailable for most regions of northwest Alaska. This study uses WorldView-2 satellite imagery to increase the spatial resolution of shallow water bathymetric data near Golovin, Alaska. Two WorldView-2 multispectral satellite images were taken in succession on September 18, 2013 GMT. The green band (510-580 nm) was found to reflect the bathymetry of the region better than the other available bands. A median filter was used to reduce noise from surface current and wave reflection, however, light impediment by suspended sediments and organics was discontinuous throughout portions of the images, and contained no relationship to the bathymetric gradient. The sensor radiance was calibrated to depth measurements taken with a single beam sonar system in July of 2012. The resultant digital elevation model (DEM) had standard errors of 0.013 and 0.006 m for the two images separately. Decorrelation of the derived depth occurred at about 3.38-3.88 m (+/- 0.43 m) below the water surface. The results of this study increased the spatial resolution of bathymetric data from the current depth measurements available on nautical charts that are approximately every 300 m, which were last made in 1900 (NOAA, 1900), to a continuous digital elevation model of measurements every 2 m.

### 3.2 Introduction

Bathymetric data provides vital information for coastal morphology, navigation, computer modeling, and seafloor mapping. The coastal zone is a location of high economic



activity that requires continuous updating of bathymetric information. Remote sensing of the bathymetry of the nearshore coastal zone would provide a continuous and easily re-measurable dataset to coastal managers. Optical sensors have often been used to infer bathymetry of shallow water coastal areas (Diedda & Sanna, 2012; Kanno & Tanaka, 2012; Lee, Olson, & Kruse, 2012; Lyzenga, 1985; Madden, 2009; Miecznik & Grabowska, 2012; Sagawa et al., 2010; Trantino et al., 2012) with reasonable accuracy.

The WorldView-2 sensor was designed to capture a portion of the optical electromagnetic spectrum more sensitive to waves transmitted through water bodies and reflected from the seafloor. The multispectral band added to the sensor used for bathymetric derivation is the Coastal Blue band (400-450 nm) (Globe, 2011). The band, in combination with other optical bands, has been used in many studies of tropical and subtropical coastal regions to detect bathymetry up to 20 m (Lee et al., 2012; Madden, 2009; Miecznik & Grabowska, 2012; Trantino et al., 2012). However, because of differences in water temperature, sediment load and bottom albedo, it is unknown if these methods would possibly be transferred to Arctic conditions.

Increased spatial resolution of bathymetry would be beneficial to populations along the Alaskan coastline. Communities in northwest Alaska experience increased water levels from storm surges. These storms cause inundation and erosion at many communities, which are built on low-lying coastal landscapes. Localized computer modeling of storm surges requires an increase in bathymetric resolution near these communities to provide much needed support for hazard preparation and management.

### 3.3 Study Area

This chapter is focused on a region surrounding Golovin, Alaska, encompassing Golovnin Bay and Lagoon (see Figure 3.1). Golovin is located on a low-lying barrier spit intersecting these two water bodies. The community is subject to flooding and erosion from storm surge events (Alaska, 2008, 2009; Blier et al., 1997; Diedda & Sanna, 2012; Kinsman & DeRaps, 2012; USACE, 2009; USGAO, 2003, 2009), but has limited and archaic (from 1900) bathymetric data available for computer modeling .

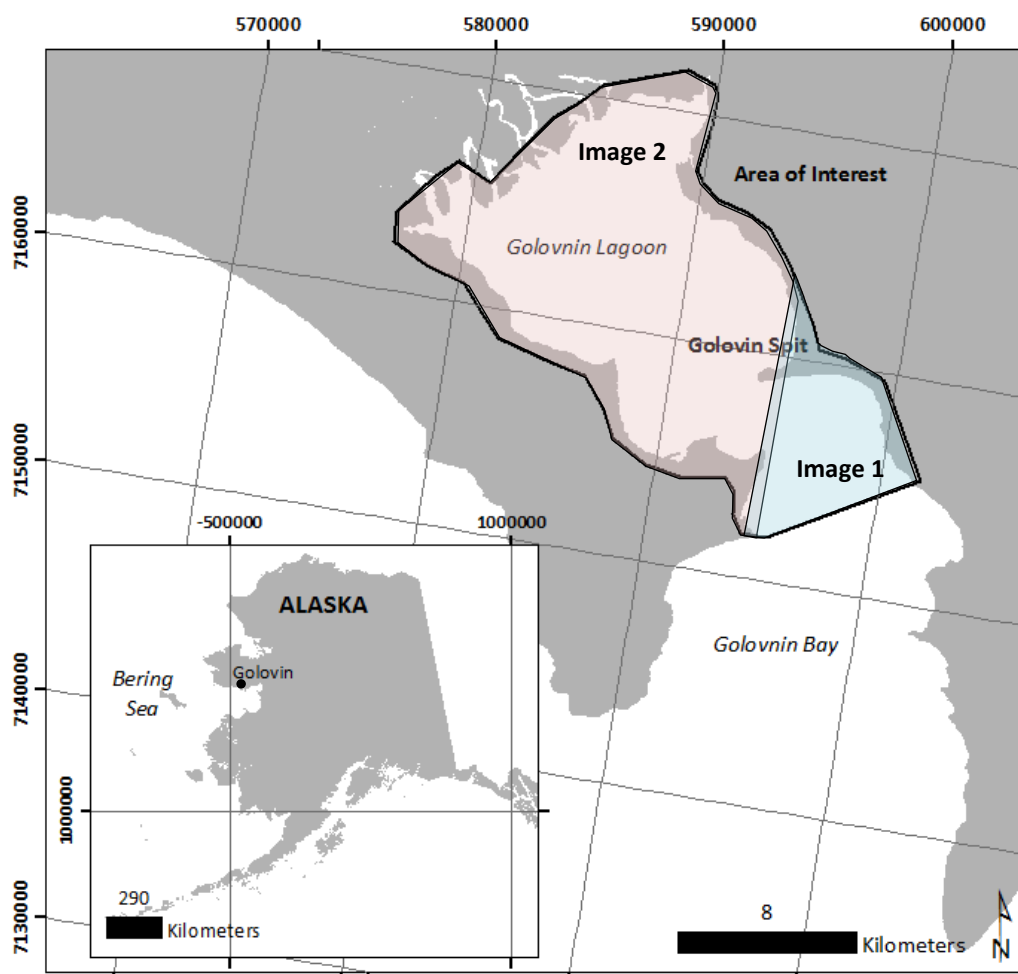


Figure 3.1—Regional map of study area relative to the state of Alaska, Image 1 and 2 shown in blue and red respectively.

### 3.4 Methods

Methods used to obtain the shallow nearshore bathymetry included integration of:

- Field measurements
- Remote sensing data enhanced by image processing

As described in the following sub-sections.

#### 3.4.1 Field Measurements

The satellite imagery was depth calibrated using surveyed measurements taken during a field excursion in July of 2012. A SonarMite single-beam sonar unit was employed to measure bathymetry at transects 0.5-1.0 km apart and 3 km long, perpendicular to the shoreline, with 2-3 transects alongshore. Most of the sonar measurements were corrected for geographic location using a TopCon HiPerII base station located onshore. Measurements taken without base station corrections were linked to locations collected with a hand held GPS unit. A tide gauge was installed during the survey to provide water elevation corrections. All measurements attained vertical accuracy of 0.46 m. Points with data quality values above 80 were used for this analysis, lower values were subject to sonar interference or non-submersion of the equipment. The sonar data were processed using SonarVista software to merge measured depths with GPS corrections, and manually edited with Fledermaus Hydro software to attain the final seafloor elevations along the ship track. All measurements were reported in elevation relative to NAVD88.

#### 3.4.2 WorldView-2 Data and Image Processing

Two WorldView-2 multispectral satellite images were taken in succession on September 18, 2013 GMT over Golovnin Bay and Golovnin Lagoon. The images were received as radiometrically correct ortho-ready products.

### 3.4.2.1 Calibration Corrections

Sensor-specific calibrations were applied using conversions available in the imagery metadata file, and used to convert the image product number to top-of-the-atmosphere radiance. Each band was converted by applying Equation 3.1 and the values in Table 3.1.

$$L_i = \frac{C_i D_i}{W_i} \quad (3.1)$$

Where  $L_i$  is the radiance recorded by the sensor ( $\text{Wm}^{-2}\text{sr}^{-1}\mu\text{m}^{-1}$ ),  $C_i$  is the absolute calibration factor ( $\text{Wm}^{-2}\text{sr}^{-1}$ ),  $D_i$  is the image product value, and  $W_i$  is the effective bandwidth ( $\mu\text{m}$ ).

Table 3.1—Calibration measures for Worldview2 satellite sensor

Band Name	Absolute Calibration Factor ( $\text{Wm}^{-2}\text{sr}^{-1}$ )	Effective Bandwidth ( $\mu\text{m}$ )
Coastal Blue	9.295654e-03	4.730000e-02
Blue	7.291212e-03	5.430000e-02
Green	5.654403e-03	6.300000e-02
Yellow	5.101088e-03	3.740000e-02
Red	7.858034e-03	5.740000e-02
Red Edge	4.539619e-03	3.930000e-02
Near Infrared 1	8.726365e-03	9.890000e-02
Near Infrared 2	9.042234e-03	9.960000e-02

### 3.4.2.2 False Reading Removal

Within each of the images, there were locations of irregular sun-glinting due to waves and other water interfaces. These locations resulted in higher than normal values for water reflectance, and were not representative of electromagnetic radiation that had reached the seafloor. Because of their irregularity, these features were removed using a median morphological filter with a kernel size of 25x25 pixels. The median filter removed false positive measurements, without changing the real measurements made by the sensor.

Other irregularities such as site-specific image striping and suspended sediments and organics were found to change the transmission of light through the water bodies. There was no physical relationship between suspended sediment and depth within the image. Because of this, portions of the image affected by suspended sediment were removed from the study by hand delineation. Some locations were highly influenced by suspended sediment, leaving large tracks of unusable data. To remove these gaps, the final data derived from the WorldView-2 imagery were combined with the original surveyed data and interpolated using a kriging interpolation across all of Golovnin Lagoon, and the entrance of Golovnin Bay.

### 3.4.3 Radiance and optical reflectance relationship

Radiance recorded by an optical sensor can be related to bottom reflectance and depth by Equation 3.2, where  $i$  denotes the sensor band (Lyzenga, 1978). This equation takes into account changes in solar irradiation as it travels through a body of water (Figure 3.2).

$$L_i - L_{si} = a_i r_i e^{-K_i z} \quad (3.2)$$

Where,  $L_{si}$  is the radiance recorded over deep water,  $a_i$  is a constant for solar irradiance,  $r_i$  is the bottom surface reflectance,  $K_i$  is the effective attenuation coefficient, and  $z$  is the water depth. For this research, the bottom surface reflectance was assumed to be homogenous, so that  $a_i$  and  $r_i$  were combined into one value. Using this equation, the effective attenuation coefficient and the combined constant for solar irradiance and bottom surface reflectance were calculated for each of the regions over the locations of known depth. These values were then applied to the entire image to calculate depth.

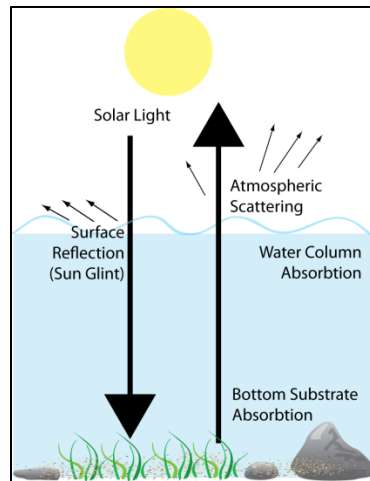


Figure 3.2—Solar radiation traveling through a body of water.

### 3.5 Results

The relationships for depth and seafloor radiance resulted in differing attenuation and bottom surface coefficients for each of the images. This is likely due to the differences in depths within the regions. The depths in Image 1 were much larger than Image 2, so these values were accepted, and the error was measured separately for each image.

The green band had the highest correlation of corrected radiance to depth value relationship, and was used to derive the bathymetry. The other bands had high volumes of noise, which made them unusable for further analysis. The bottom surface coefficients and their 95% confidence intervals were found to be 8.544 (+/- 0.073) and 1.984 (+/- 0.024), with attenuation coefficients of -0.6840 (+/- 0.0084) and -0.8421 (+/- 0.0175) for Image 1 and 2 respectively (see Figures 3.3 & 3.4). These relationships were used to calculate the depths of all pixels in both scenes, which are shown in Figure 3.5.

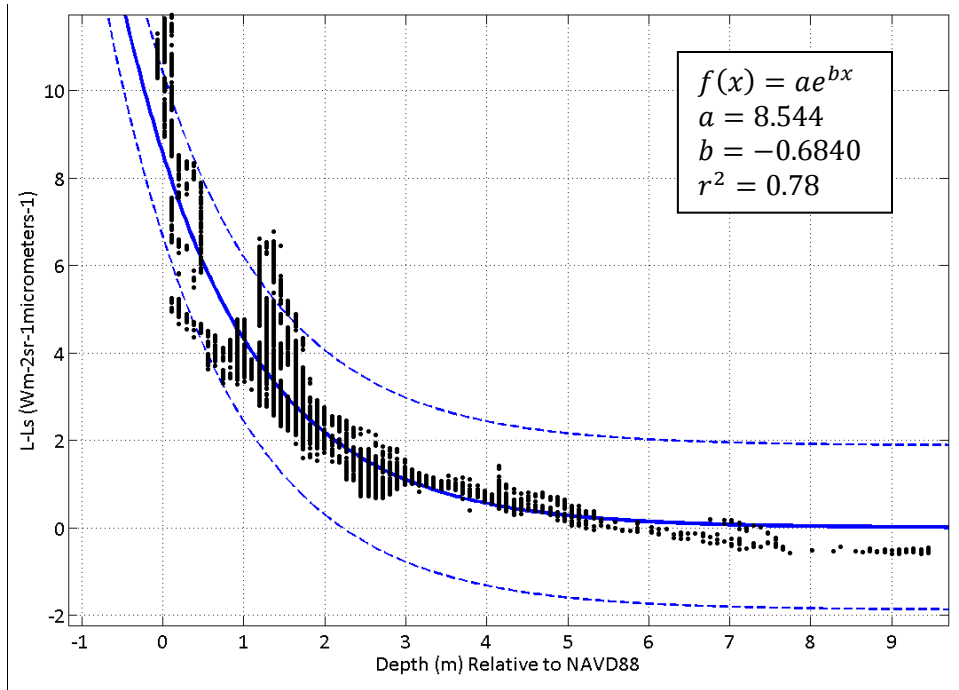


Figure 3.3—Exponential relationship of measured depth relative to sensor radiance for Image 1, with 95% confidence interval.

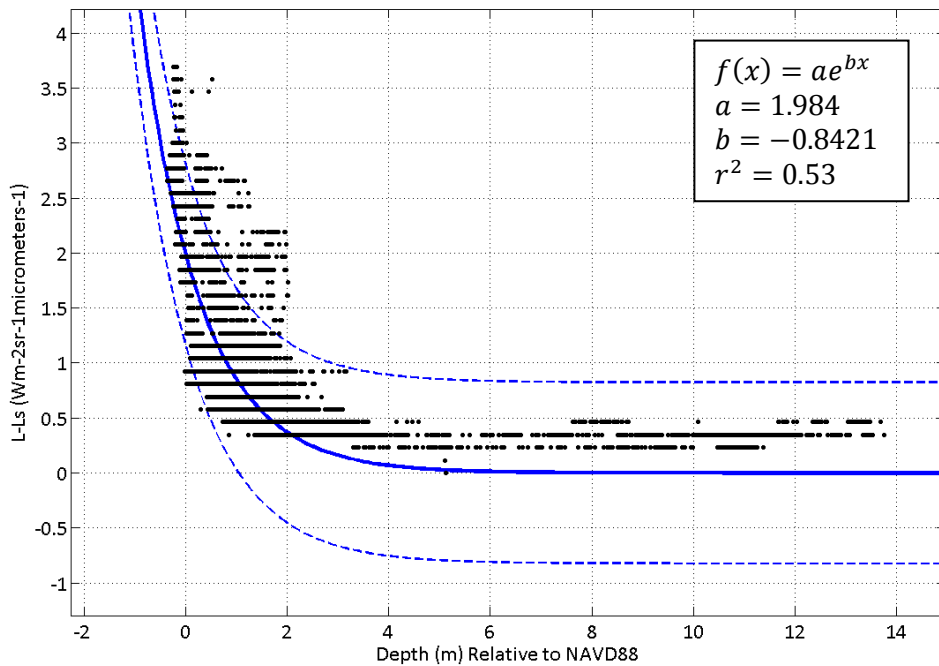


Figure 3.4—Exponential relationship of measured depth relative to sensor radiance for Image 2, with 95% confidence interval.

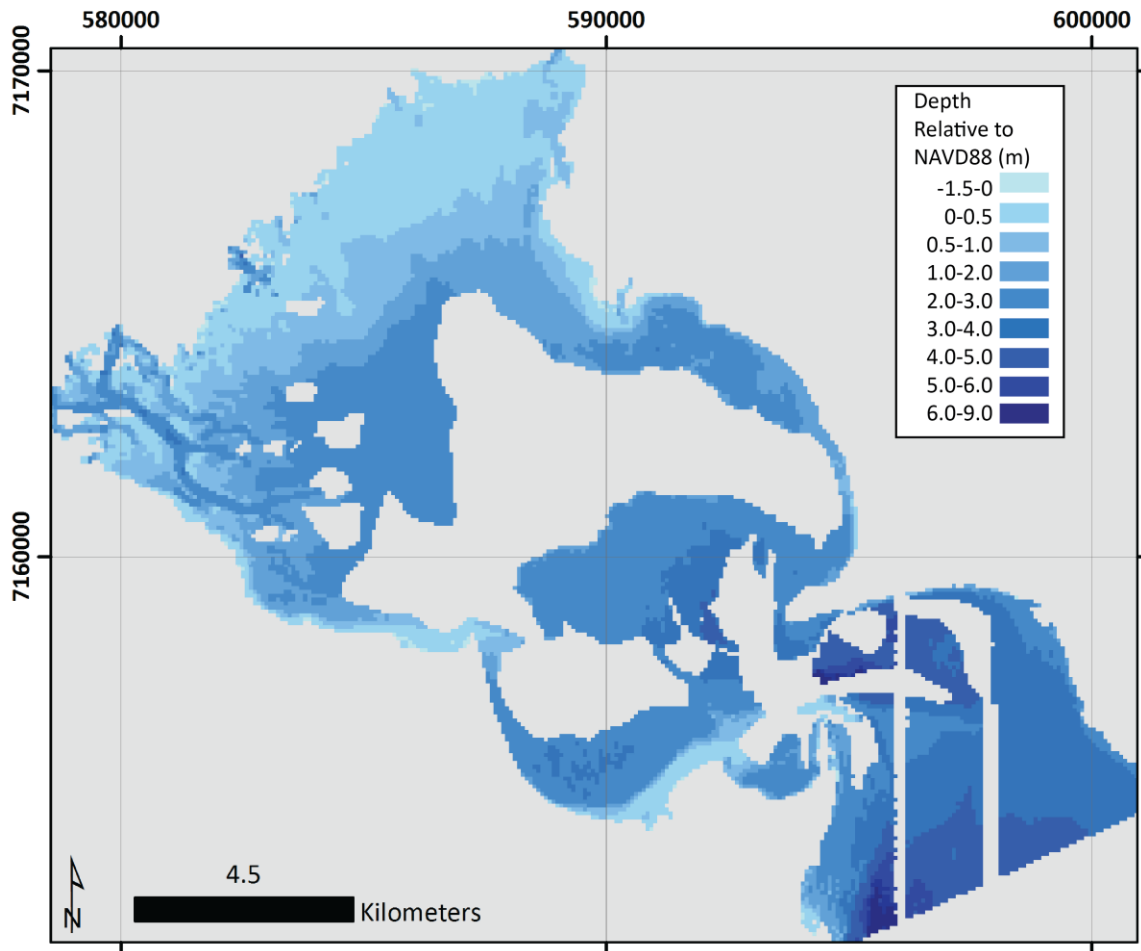


Figure 3.5—Classified bathymetric map of Golovnin Bay and Golovnin Lagoon, missing data/background in gray, projected in NAD83 UTM Zone 3N, on the NAVD88 vertical datum, pixel size of 80 m.

The resultant DEM, although missing swaths, was interpolated and used for numerical modeling (Figure 3.6). The analysis predicted depth variation at river channels, as well as low gradient changes in the mapped portion of the lagoon. The offshore bar system south of Golovin, was also reflected in the measurements, with an updated shape compared to previous nautical charts. The large portions of data missing within the lagoon covered regions with



minimal fluctuations in depth based on the current nautical charts, which made the interpolation a reasonable assessment of bathymetry.

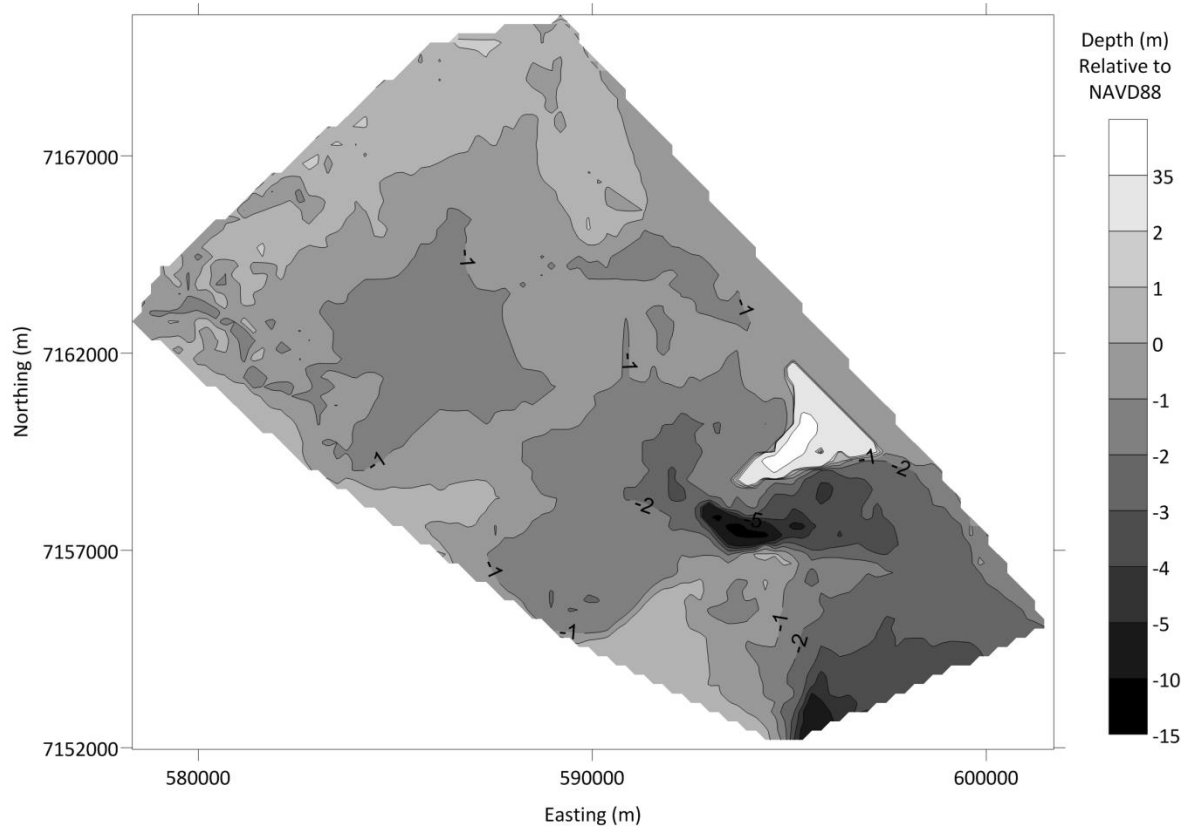


Figure 3.6—Interpolated bathymetry using WorldView-2 and surveyed data, projected in NAD83, UTM Zone 3N, datum in NAVD88.

Measured values corresponded to the satellite-predicted values. The measured and predicted values were plotted relative to a 1:1 relationship in Figures 3.7 and 3.8. The standard error was calculated between all measured and predicted values, and was found to be 0.013 m for Image 1 and 0.006 m for Image 2.

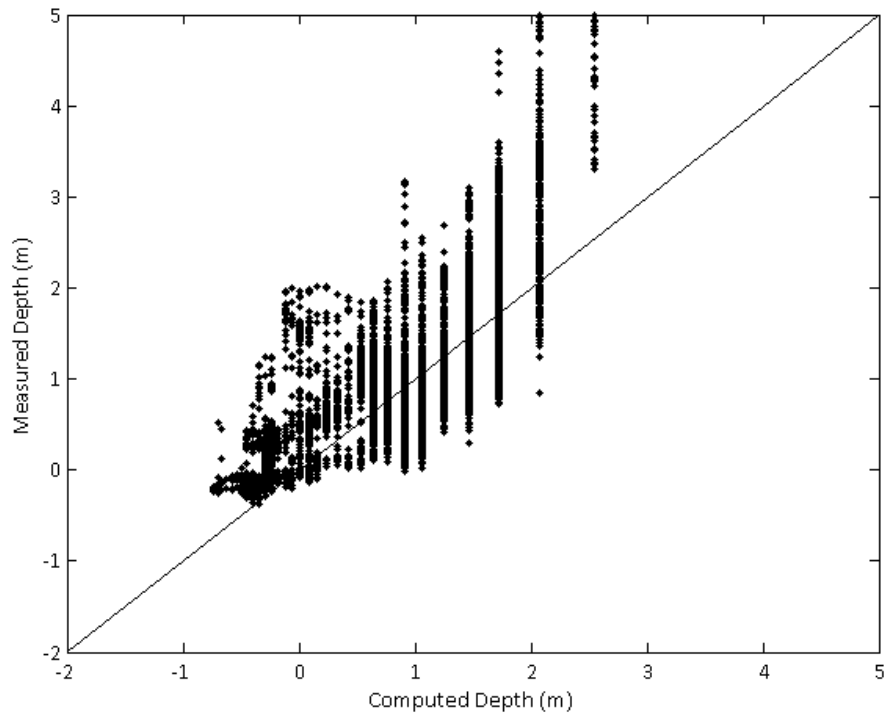


Figure 3.7—Measured vs computed depths for Image 1 (total points=9560), relative to 1:1.

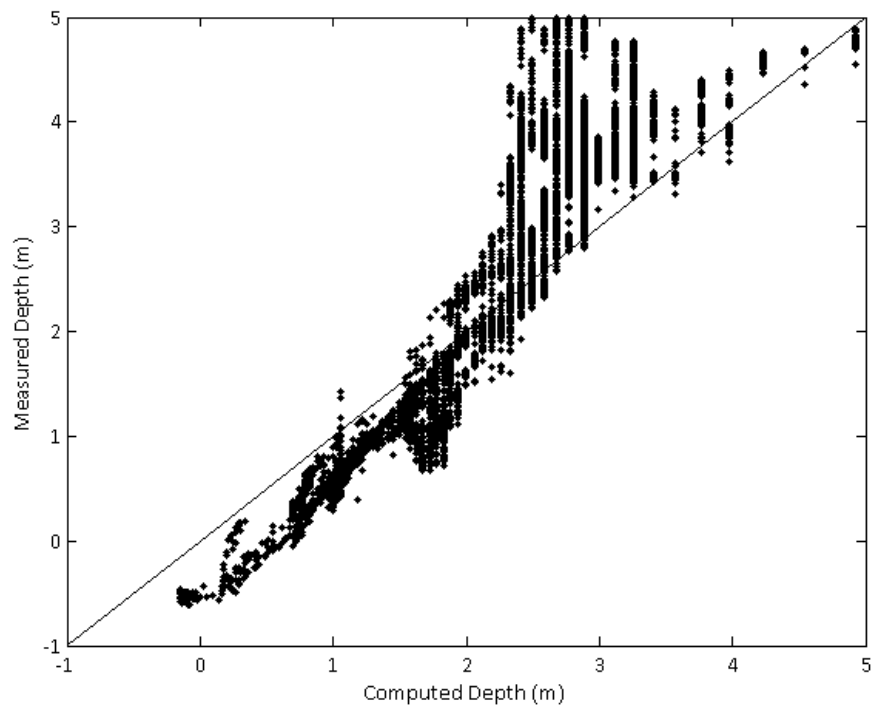


Figure 3.8—Measured vs computed depths for Image 2 (total points=8768), relative to 1:1.

### 3.6 Discussion & Conclusion

Data acquired with the WorldView-2 sensor was used to determine the depth of water in Golovnin Bay and Lagoon. The depths were predicted from the measured image radiance calibrated to measured depth values taken in July of 2012. The coefficients of bottom substrate reflectance and attenuation were derived from this relationship (R-squared values of 0.78 and 0.53). The standard error between measured and derived depth values were 0.013 and 0.006 m, which is reasonable for the depth measurements which ranged from -1.5-9 m.

The green band was shown to best reflect the variation in seafloor depth for this location. All other bands were found to have a large volume of noise over the water surface. This was likely due to the reduced incoming solar irradiance at the time of year the images were procured. The images used for this analysis were procured in September of 2013, when solar irradiance is decreased compared to summer conditions in arctic and sub-arctic regions, which reduced the potential energy entering the observed water bodies. The water in this region was also colder and therefore denser than that of tropical regions, which could have reduced the amount of solar irradiance transmitted through the water. The bottom substrate was also darker than that of tropical regions, reducing the albedo and therefore the reflection of light even further. However, for the nearshore region around Golovin, the depth was reasonably determined.

Large swaths of the study area were subject to changes in light transmission due to suspended organics and sediments. In the locations with both suspended sediment and measured bathymetry, no relationship was found between seafloor irradiance and measured depths. The sediment did not allow the solar radiation to transmit through the water column, and the water depth did not control the amount of suspended sediment in the water column.

For these reasons, these locations were not analyzed using the methods of this research. Other locations, such as Wales, Alaska, are subject to different mechanisms of sediment transport in the nearshore. The reflectance of sediment transported in longshore bars were found to correspond to depth in WorldView-2 imagery (Smith, Kinsman, & Misra, 2013). These differences in the mechanisms of sediment transport are significant for future applications of this method.

The correlation between measured and derived bathymetry was shown to decrease with depth in both images. The decorrelation began at about 2 m for Image 1 and 2.5 m for Image 2. This may be representative of a threshold limitation of bathymetric surveying in this region. These values correspond to an average of 3.88 m depth ( $\pm 0.43$  m tidal range), below the water surface. Depths within this boundary are still very important to hydrodynamic models, but do create limitations to this study. The combination of data derived from WorldView-2 satellite measurements and measured bathymetric data were used to create a bathymetric grid for numerical modeling.

With the launch of the Landsat 8 OLI/TIRS satellite, more freely available multispectral data may begin to become available for coastal regions of Alaska. Future work should include this type of imagery, because of the reduced cost to the end user and the similarity in spectral resolution to that of the WorldView-2 sensor. Reduction in spatial resolution may affect accuracy; however, the resulting DEM would be an upgrade to that which is currently available for most regions.



## **Chapter 4 Numerical Modeling of Coastal Morphodynamics in Response to Extreme Storm Events on the Golovin Barrier Spit in Northwest Alaska**

### 4.1 Abstract

Golovin, Alaska, is located on a low-lying barrier spit subject to episodic flooding and erosion as a result of recurrent storm surges. The objective of this research is to use XBeach models to assess maximum inundation and erosion adjacent to community infrastructure and support planning of future preventative measures to these hazards. XBeach is a one-dimensional process-based hydrodynamic model designed for morphological response and maximum water level predictions of nearshore storm events. Cross-shore profiles at five locations on the spit were modeled for five differing storm conditions based on 5-100-year recurrence intervals. The model results illustrated that sediments were transported from the beach face to a nearshore bar rather than permanently offshore. Maximum runup elevations exceeded input water elevations by as much as 1.04 m on the bay side of the spit, with the potential for runup on the lagoon side of the spit to 1.08 times greater than the runup on the bay side of the spit. The model results indicated a need for flood prevention structures at Golovin but not shoreline stabilization to remediate erosion. These modeled heights may be used in the engineered design of a levee for long-term prevention of flooding or applied to differing storm water elevations for temporary berm designs. The effects of the frozen landscape were not included in this research, but may be critical in engineering designs and could change model outcomes. Hence, the effects of freezing and thawing of the nearshore and beach environment should be considered in future analyses.

## 4.2 Introduction

The nearshore coastal zone is not only a highly dynamic environment dependent on hydrodynamics and geology; it is a zone of high economic activity and development in most regions of the United States. In Alaska, particularly northwest Alaska, this is also the case. Although coastal populations are much smaller than cities in coastal regions of the lower U.S., the economic value of the region and the density of human infrastructure on low-lying features make communities within the region vulnerable to potential coastal geohazards such as flooding and erosion. The lack of hydraulic data and regular monitoring systems makes engineering design of remediation structures costly. To reduce uncertainties, we must reduce the spatial resolution of hydrodynamic models and apply them to specific vulnerable communities, separately. This would provide the best estimation of coastal vulnerability to hydrodynamic processes on a community-by-community basis.

Morphological hydrodynamic models are used by coastal scientists and engineers to perform large volumes of calculations using a suite of physical variables to determine the potential for sediment redistribution in the nearshore coastal zone. XBeach is a one-dimensional finite-difference wave propagation model developed by the USACE, UNESCO-IHE, Deltares, Delft University of Technology, and the University of Miami (Roelvink et al., 2010). The model is based on a classification system developed by Sallenger (2000) for barrier island response to storm surge, which includes beach response to varying water and wave height relative to the dune surface, including: swash, collision, overwash, and inundation (Figure 4.1). The model is best used for single event small spatial scale modeling for events no longer than 11 days (Roelvink et al., 2010). The model accounts for short wave envelope propagation, non-stationary shallow water equations, sediment transport, and bed updates (Roelvink et al., 2010). The model has

been validated in multiple coastal environments for differing storm conditions (Roelvink et al., 2009; Vousdoukas, Almeida, & Ferreira, 2011) and provides a best estimate for maximum water elevations and sediment redistribution without overcomplicating the input parameters. This is optimal for northwest Alaska, because of the paucity of oceanographic data. Although reductions in model uncertainty could be achieved by expanding to two or even three dimensions, simplifying the model allows for expediency in the process and transferability to other locations within the region.

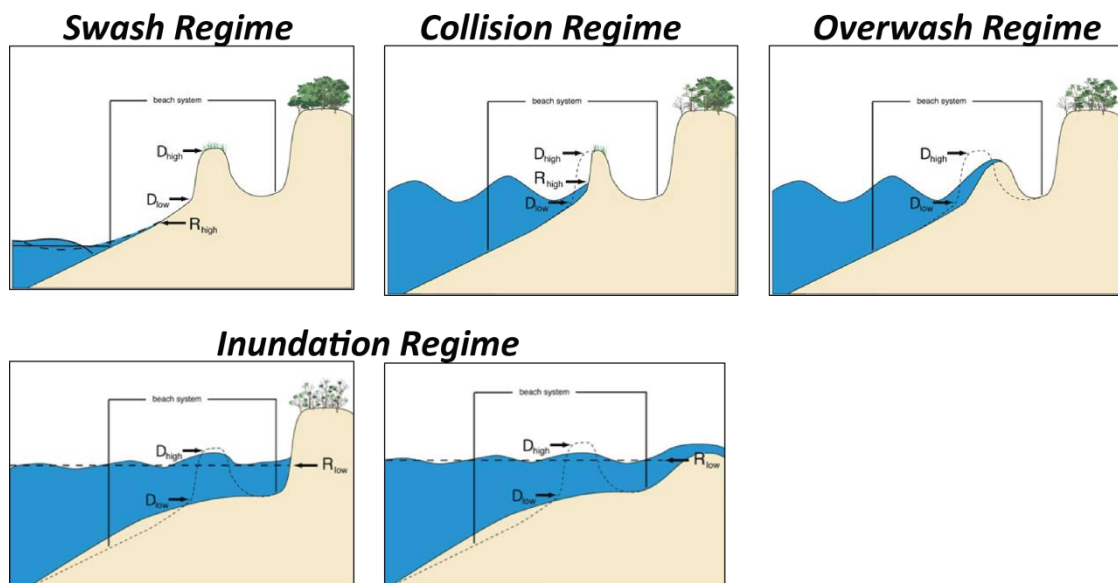


Figure 4.1—Four regimes of storm impact on the barrier environment (Sallenger, 2000), reproduced from USGS (2013).

## 4.3 Methods

### 4.3.1 Model Setup

Five storm water elevations, modeled by the USACE as events from 5-100-year return interval storms, were modeled at five profiles located approximately 250 m apart along the



Golovin spit (Figures 4.2 and 4.3). Each storm was limited to 30 hours (108000 seconds), with linear storm hydrographs peaking at 15 hours. The beach and ocean were assumed to be in non-frozen conditions, because of the lack of modeling software available to address these issues.

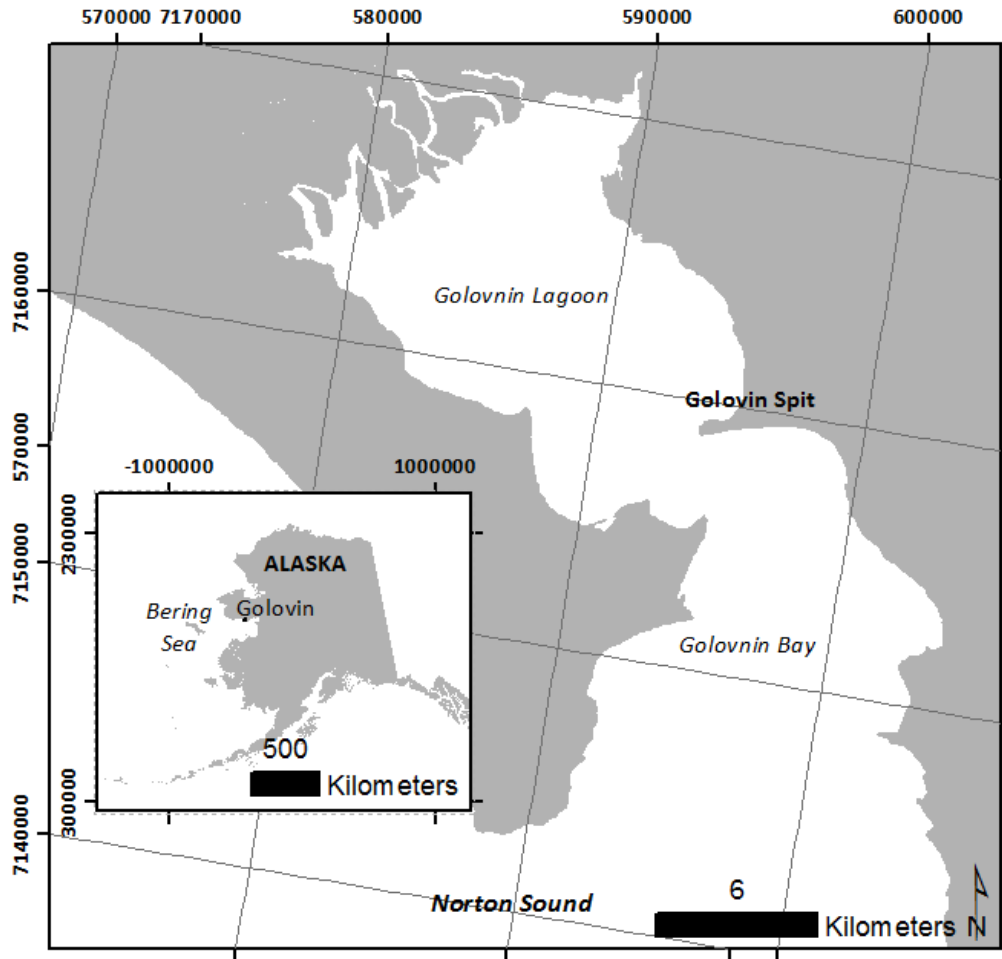


Figure 4.2—Regional map of study location, zoomed-in data is projected in NAD83 UTM Zone 3N, zoomed-out data is projected in NAD83 Alaska Albers.



Figure 4.3—Alongshore locations of profiles modeled, projected in NAD83 UTM Zone 3N on panchromatic WorldView-2 image.

#### 4.3.1.1 Model Domain

The grids for each of the model computations were created using surveyed elevations and the best data layer for bathymetric depths. Beach elevations were collected in July 2013 from a real-time-kinematic survey. The bathymetry used in the modeling was derived from calibrated WorldView-2 multispectral imagery and bathymetry measured during a sonar survey in July 2012. The model profiles were extended offshore to approximately 7 km, oriented perpendicular to shoreline at the five profiles along the bay side of the Golovin spit. The vertical datum was converted from all other vertical references to elevation zero at mean tide level (MTL). Irregular grid spacing was used in Open Earth Tools XBeach toolbox, with larger grid spacings further offshore and smaller grid spacings on the beach face.

#### 4.3.1.2 Hydrodynamic Conditions

The USACE developed a region-wide storm surge model in 2009 in support of continued projects in 17 communities of northwest Alaska, including Golovin. The Advanced Circulation model for oceanic, coastal and estuarine waters (ADCIRC) was calibrated to water surface elevations from storm events recorded on October 2004 and October 1992 at the Nome and Red Dog gauging stations (Chapman et al., 2009). 52 historical storm events were run in the ADCIRC model, and a frequency-of-occurrence relationship was generated based on the empirical simulation technique (Chapman et al., 2009). The water elevations resulting from the analysis define the maximum offshore water elevations for the models in this study (Table 4.1).

Table 4.1—Modeled storm heights at Golovin (Chapman et al., 2009).

Return Period (years)	Storm Water Elevation (m MLLW*)	Standard Deviation (m)
5	1.83	0.23
10	2.44	0.26
25	2.99	0.37
50	3.68	0.82
100	4.46	1.03

\*Mean lower-low water (MLLW)

Offshore wave heights have also been modeled for a region near Golovin by the USACE using the WAM Cycle 4.5 wave model, through the wave information studies online database (USACE, 2013). The same return interval used to determine storm elevation was input into the modeled relationship derived by the USACE, to determine the significant wave height ( $H_{mo}$ ) for station 82124, (Equation 4.1) located offshore and outside of Golovnin Bay.

$$H_{mo} = 2.7585 + 0.59218 \ln(R) \quad (4.1)$$

Where  $R$  is the return interval in years. From the significant wave height, the Peirson-Moskowitz parameters for wind velocity and peak frequency ( $f_p$ ) were back-calculated (Sorensen, 2006):

$$H_{mo} = 0.21 \frac{W^2}{g} \quad (4.2)$$

Where  $W$  is the wind speed (m/s), and  $g$  is the gravitational acceleration (m/s<sup>2</sup>).

$$f_p = \frac{0.87g}{2\pi W} \quad (4.3)$$

The results were directly input into the wave characterization files and are summarized in Table 4.2. All wave spectra were given one significant wave height applied to a Joint North Sea Wave Project (JONSWAP) spectrum for the entire run of each model. The methodology for determining wind speed was validated for a storm in October 2013. Wind speed measured at the local airport was compared to calculated wind speed using the above equations and found to be the same (12.5 m/s).

Table 4.2—Empirically derived wind speed and wave frequency based on mean wave height.

Return Interval (years)	Significant Wave Height (m)	Wind Speed (m/s)	Peak Wave Frequency (s <sup>-1</sup> )
5	3.71	13.15	0.103
10	4.12	13.90	0.098
25	4.66	14.75	0.092
50	5.08	15.40	0.088
100	5.50	16.03	0.085

Wind, and therefore, wind-driven-wave direction was determined using the storms modeled by the USACE from the ten highest predicted storm events at Golovin (Chapman et al., 2009). Since the wind direction was not related to storm height, the weighted average of all values was used as the wind and wave direction for each of the profiles in all storm conditions (191.25° from North).

Astronomical tide effects were not included in the model analysis, the astronomical tide was assumed to be at the local mean tide level for the duration of the model runs. This

simplification was employed because of the minimal tidal range (0.43 m) and the unknown time to which they would have occurred during any given storm event. Since the tides are diurnal at Golovin, tidal influence would be expected throughout a storm event, but would be minimal relative to the increased storm water elevations and wind waves.

#### 4.3.1.3 Beach Sediments

The XBeach model allows for only one value of sediment size to be used for computation. Values of  $D_{50}$  and  $D_{90}$  were measured at locations across each profile, on the beach face. These values were then averaged to compute the overall sediment sizes of each profile (Table 4.3). For further information refer to the methods described in Chapter 1.

Table 4.3—Grain size values used for model purposes.

Profile	$D_{50}$ (mm)	$D_{90}$ (mm)
1	1.30	1.44
2	2.50	4.03
3	1.52	2.63
4	1.96	3.30
5	3.94	6.44

#### 4.3.1.4 Calibration & Validation

The model was calibrated using field survey data from July 2013 and October 2013. Coastal profiles were measured before and after a small scale storm event (calibration storm) that passed over Golovin. Measurements of the hydrodynamics of the calibration storm were attempted using a Nortek acoustic wave and current profiler; however, we were unable to retrieve the equipment and this data was not available for use in this model. Because of this, significant wave height and peak frequency were extrapolated from the same frequency-of-occurrence model used to describe the wind and wave hydrodynamics, based on the wind speed collected at the local airport. A maximum water level was measured on the lagoon side of the

spit to 1.232 m above MTL on October 26, 2014 (Figure 4.4). This water level was enhanced by the outflow of water from the bay bottleneaking at the spit, so this value served as the maximum possible storm water elevation.



Figure 4.4—Maximum water level measured by Alexander Gould.

From the maximum possible storm water elevation, storms of increasing water elevations, to 1.232 m were modeled on Profile 1 and compared to the surveyed measurements (Figure 4.5). The offshore calibration storm elevation with similar vertical translation of beach sediments was 0.65 m above MTL. The amount of vertical displacement of sediment was within 1.6 cm at 1 m elevation and 3.9 cm at 2 m elevation (above MTL) in comparison to the measured values (Figure 4.6). These were considered to be reasonable estimates based on the simulation and the vertical displacements measured in the field (October 26, 2013).

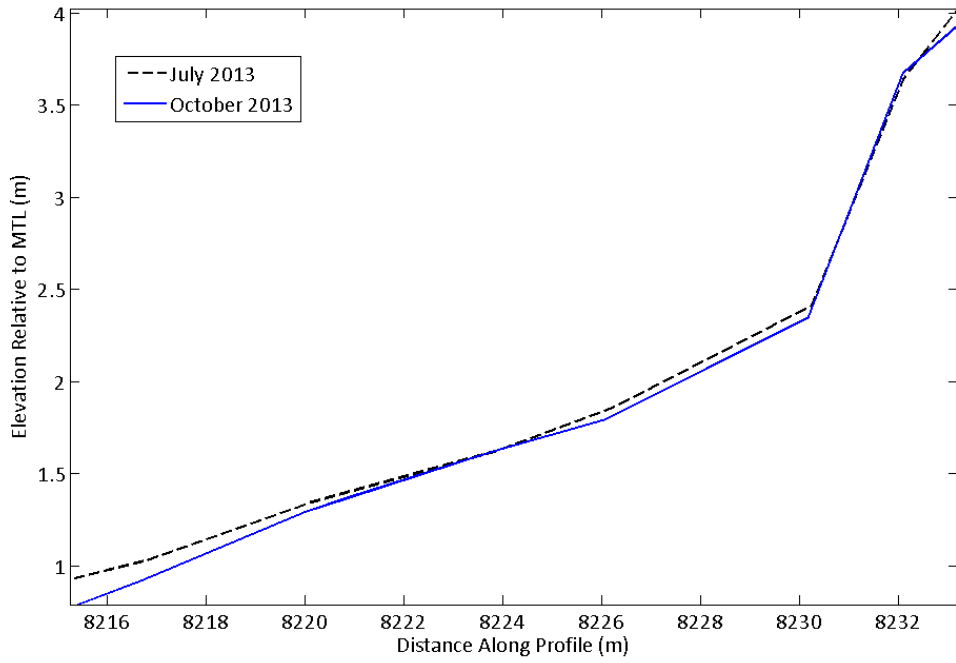


Figure 4.5—Measured Profile 1 before and after calibration storm event.

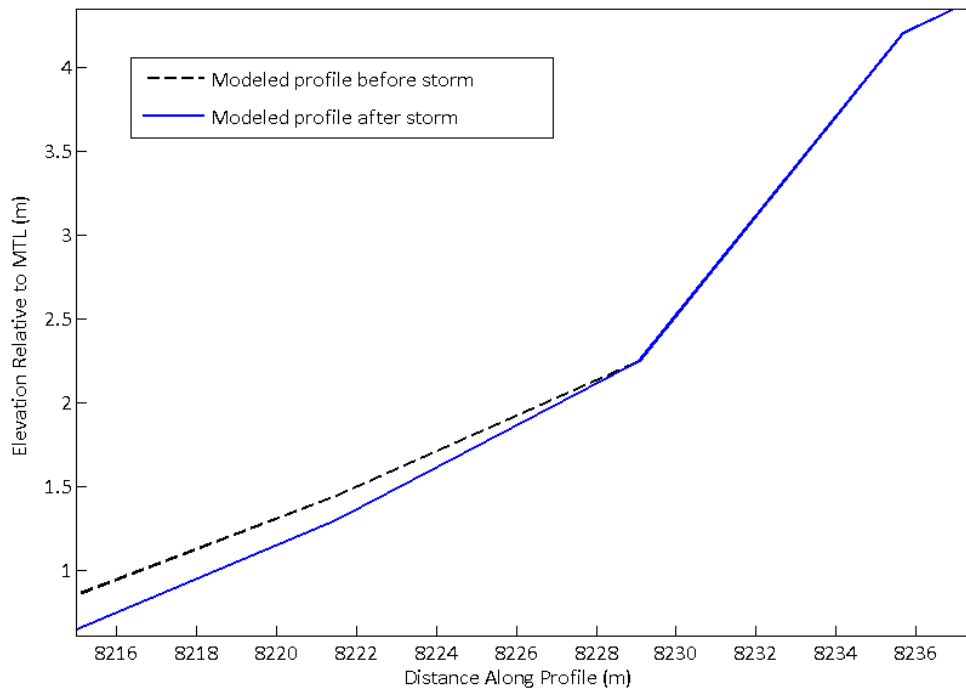


Figure 4.6—Modeled Profile 1 before and after calibration storm event.

After calibrating the offshore maximum storm water level, parameters were tested for their sensitivity. The parameters tested were the breaker slope coefficient ( $\beta$ ), the calibration factor for time-averaged flows due to wave skewness and asymmetry ( $\text{facau}$ ), and the critical avalanching slope under water ( $\text{wetslp}$ ), described by Roelvink et al. (2009) and Vousdoukas et al. (2011) as the most sensitive to model inputs. The  $\text{wetslp}$  and  $\text{facau}$  parameters were found to change the erosive morphology of the beach after the storm, however, when tested at variable values, at differing offshore storm elevations, they were unable to produce the measured profile. Therefore, these parameters were left as their default values for the subsequent modeling efforts. Vousdoukas et al. (2011) also suggested turning off the wave-current interaction ( $\text{wci}=0$ ) and using the Vanthiel-Van Rijn equations for equilibrium sediment concentration formation for steep beaches, which was used in this analysis.

#### 4.3.2 Flooding Projections

Because of the shape of Golovnin Lagoon, flood waters that enter the lagoon must also exit through a constricted channel. The constricted water piles up on the lagoon side of the spit, increasing the inundation elevation beyond the maximum expected storm water elevation. The maximum runup elevations on the bay side of the spit corresponded to higher runup elevations on the lagoon side of the spit. These values were measured for two separate storm events, the calibration storm from October 2013, as well as a storm that occurred in November 2011, measured by the Alaska DGGS (Kinsman & DeRaps, 2012). A linear relationship was defined between the runup on the bay and lagoon sides of the spit (passing through the origin to correspond to zero runup on the lagoon side with zero runup on the bay side), resulting in a setup factor for the lagoon side of the spit (Equation 4.4). Since the lagoon side is not only



inundated to higher elevations, but also has lower berm elevations on the beach face, maximum runup values are important for this portion of the spit.

$$R_L = 1.08 R_B \quad (4.4)$$

Where  $R_L$  is equal to the runup on the lagoon side of the spit, and  $R_B$  is the runup on the bay side of the spit. This relationship allows for a form of storm setup to be including in flood mapping on the lagoon side of the spit, but is subject to error. The linear relationship resulted in an r-squared value of 0.9988. However, only two values were used to define the relationship here, if more measurements are made in the future, more points can be used to improve the setup factor and to determine if the relationship is linear or not.

#### 4.4 Results and Discussion

The maximum water elevations in Table 4.4 are representative of the total water level at the coastline, including runup and assuming a negligible astronomical tide. When maximum runup values on the bay side of the spit were confined to the beach face, the values were similar along the spit (at all profiles), which corresponded to the 25-year storm event (Figure 4.7). However, when runup reached the backshore and beyond, maximum runup corresponded to the slope of the surface beyond the backshore. This difference in runup was as much as 0.6 m for the 100-year storm. The runup induced by the 25-year storm may be indicative of a threshold storm, beyond which, water elevations induce overwash and inundation of the central part of the spit. The 50-100-year storms were resulted in overwash of the entire spit, both from flooding on the bay and lagoon sides. Some sediments were transported landward during these storms resulting in increased in the surface elevation beyond the beach face.

The maximum water elevations, modeled here, were above normal conditions, which were not reflected in the current grain size distributions on the spit. This likely corresponds to

rapid recovery of the beach to storm events. However, since flooding occurs at irregular intervals and is not measured at Golovin, heights of the most recent increases in water elevations above the beach face are unknown.

Table 4.4—Modeled maximum water elevations and sediment redistribution at each profile for each storm (maximum water elevation is runup, sediment loss at the vegetation line is the maximum vertical translation of sediments due to erosion, and the sediment added to back is the increase in the sediment surface beyond the beach face due to overwash).

Return Interval (years)	Profile 1		Profile 2		Profile 3			Profile 4			Profile 5		
	Max Water Elev. (m)	Sed Loss at Veg (m)	Max Water Elev. (m)	Sed Loss at Veg (m)	Max Water Elev. (m)	Sed Loss at Veg (m)	Sed Added to back (m)	Max Water Elev. (m)	Sed Loss at Veg (m)	Sed Added to back (m)	Max Water Elev. (m)	Sed Loss at Veg (m)	Sed Added to back (m)
5	2.574	-1.94	2.57	-1.37	2.09	-1.27	0.00	2.45	-0.85	0.00	2.40	-0.82	0.00
10	3.28	-2.06	3.27	-2.46	2.88	-1.60	0.00	2.80	-1.23	0.00	3.09	-1.35	0.00
25	4.05	-2.43	3.89	-3.19	4.06	-1.72	0.14	3.91	-1.47	0.07	3.97	-1.69	0.05
50	4.39	-2.63	5.01	-4.30	4.09	-1.83	0.41	4.13	-1.37	0.02	3.97	-1.68	0.68
100	4.87	-2.86	5.49	-4.45	4.81	-1.88	0.33	4.71	-1.45	-	4.68	-1.73	0.73

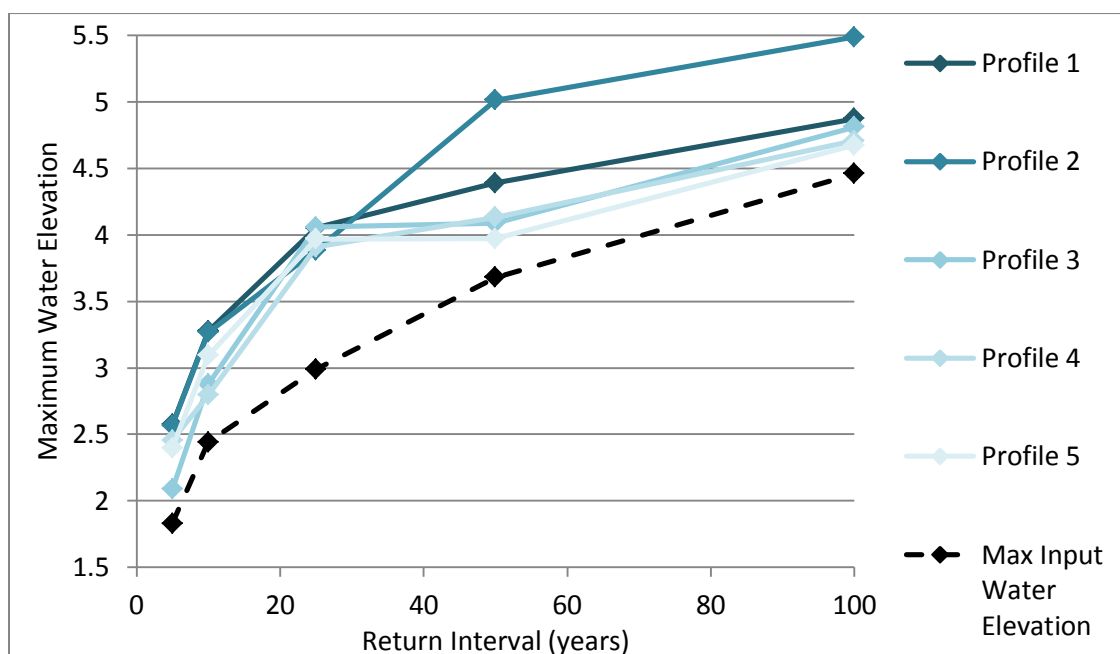


Figure 4.7—Maximum water elevation at the shoreline at each profile, compared to inputs.

The modeled values for runup were slightly higher than the original storm elevation predictions by USACE, which was expected because of the increases in water elevations that occur as they approach the coastline from an offshore position. The elevated water surface during a storm event was calibrated to measured values on the lagoon side of the spit and compared to measured values from 2011 to establish a linear relationship in flooding on both sides of the spit. The increases in water elevations were calibrated to 1.08 times greater on the lagoon side compared to the bay side. The original offshore storm water elevations are shown in Table 4.5 with corresponding flooding predictions for the lagoon side of the spit. These values may be used as design water elevations that take into account all changes in water elevations as a storm propagates towards the shoreline, on both the bay and lagoon side of the spit.

Table 4.5—Inundation extents on the lagoon side of the spit.

Return Period (years)	Surge Level (m MTL)	Runup Elevation on the Lagoon Side (m MTL)
5	1.83	2.61
10	2.44	3.31
25	2.99	4.29
50	3.68	4.66
100	4.46	5.30

Beach face elevations were translated vertically downward at each of the profiles in the modeled storm events (Figures 4.8-4.12). The vertical translation was considered to be erosion, and was maximized near the vegetation lines (Table 4.4 and Figure 4.13). Sediment transported from the beach face to the nearshore, is not likely permanent erosion, but a temporary change at each profile (Komar, 1998). Sediments in the nearshore would be transported back to the beach face during seasons of lower wave energy. This process would be consistent with the

present of the large nearshore bar system extending from the opposite coastline. This bar system not only reduces wave energy experienced at the coastline, but holds sediments within the system, by reducing bedload transport.

Downward vertical translation near the vegetation line resulted in decreases in beach slope at all of the profiles (Figures 4.8-4.12) after the 25-year storm event. This change is the result of the beginning of the transition in erosion mechanisms from collisional to overwash regimes. Since the sediments are likely to be transported back to the beach face during lower energy hydraulic environments, these changes aren't expected to affect the long-term slope of the beach. However, if storms become more frequent, these sediments may not be able to recover in this way between subsequent high energy events. Also, reductions in beach slope over time would reduce the reflectivity of the beach to hydraulic energy, which corresponds to more energy available to increase runup elevations.

The maximum values for vertical translation at the vegetation line occurred at profiles with higher elevations beyond the beach (Profiles 1 and 2) (Figures 4.8, 4.9, and 4.13), likely because of the larger sediment supply available to be eroded. Vertical translation at the vegetation line at the shallower dipping profiles (Profiles 3-5) (Figures 4.10-4.13) was similar for each storm event, and was not increased dramatically after the 25-year storm, indicating a threshold (similar to runup and changes in slope) of erosion at the vegetation line during this 25-year storm event for these profiles.

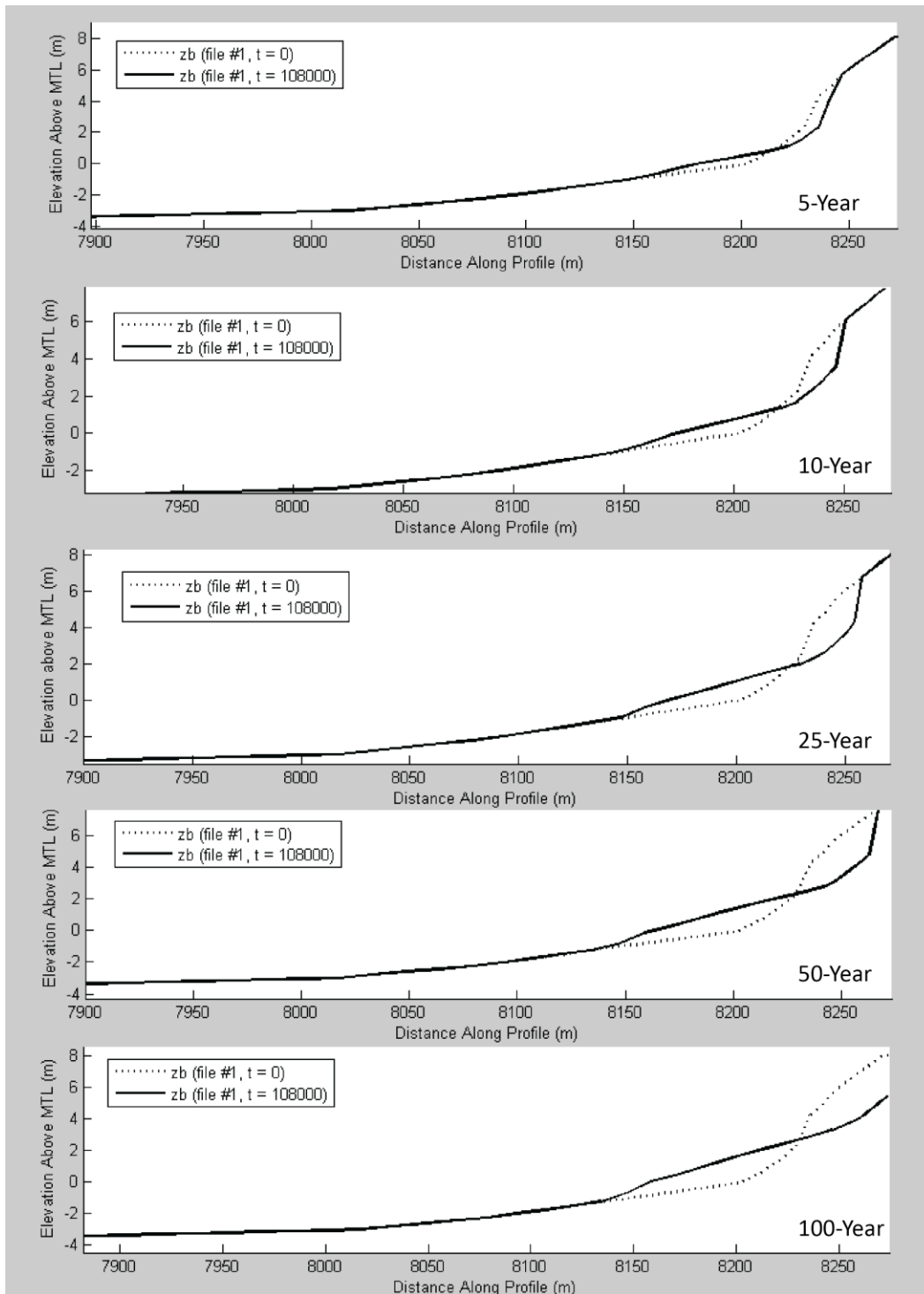


Figure 4.8—Profile 1 morphological changes with varying storm frequency of 5, 10, 25, 50, and 100 years, from time 0 to time of 108000 seconds.

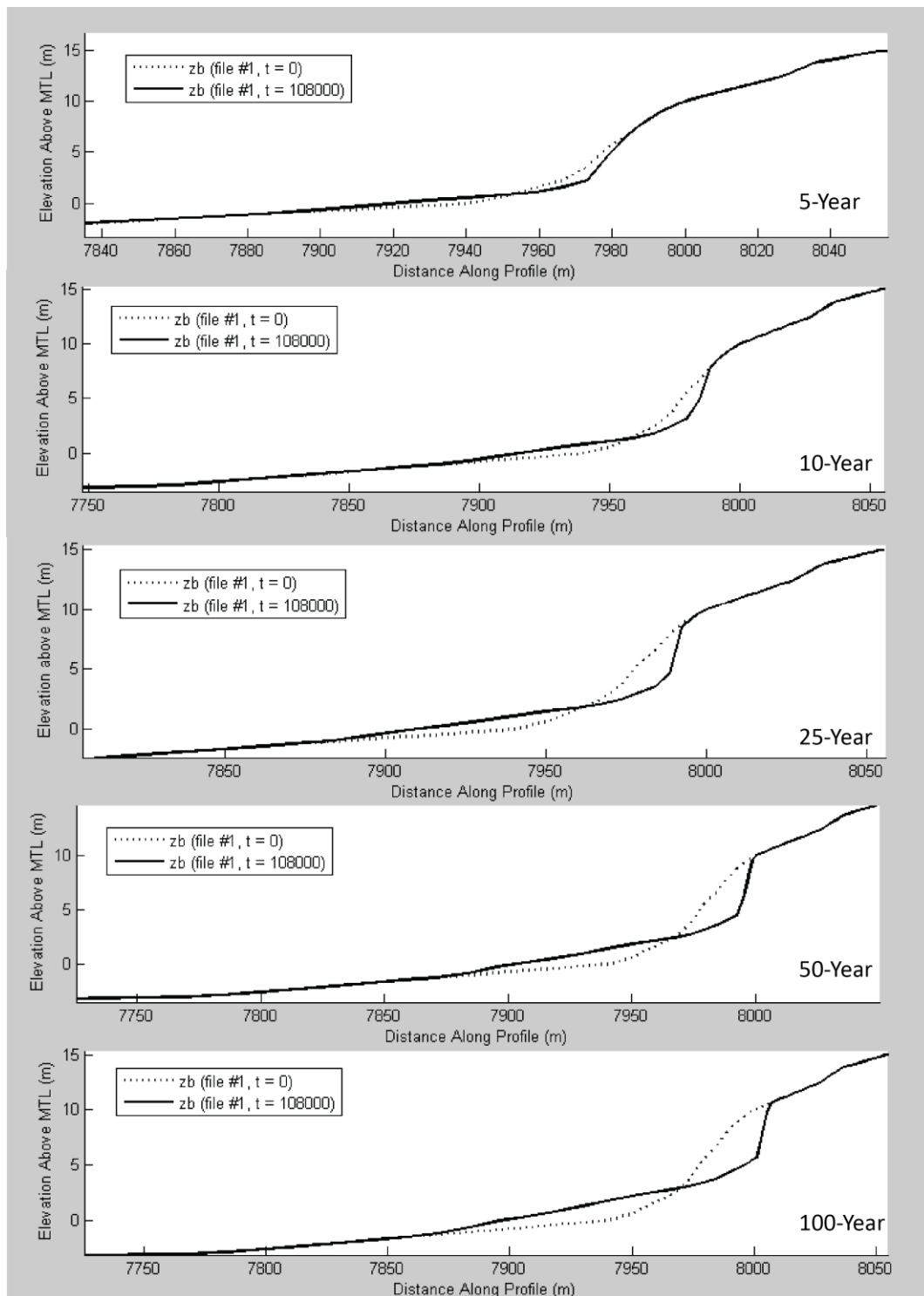


Figure 4.9—Profile 2 morphological changes with varying storm frequency of 5, 10, 25, 50, and 100 years, from time 0 to time of 108000 seconds.

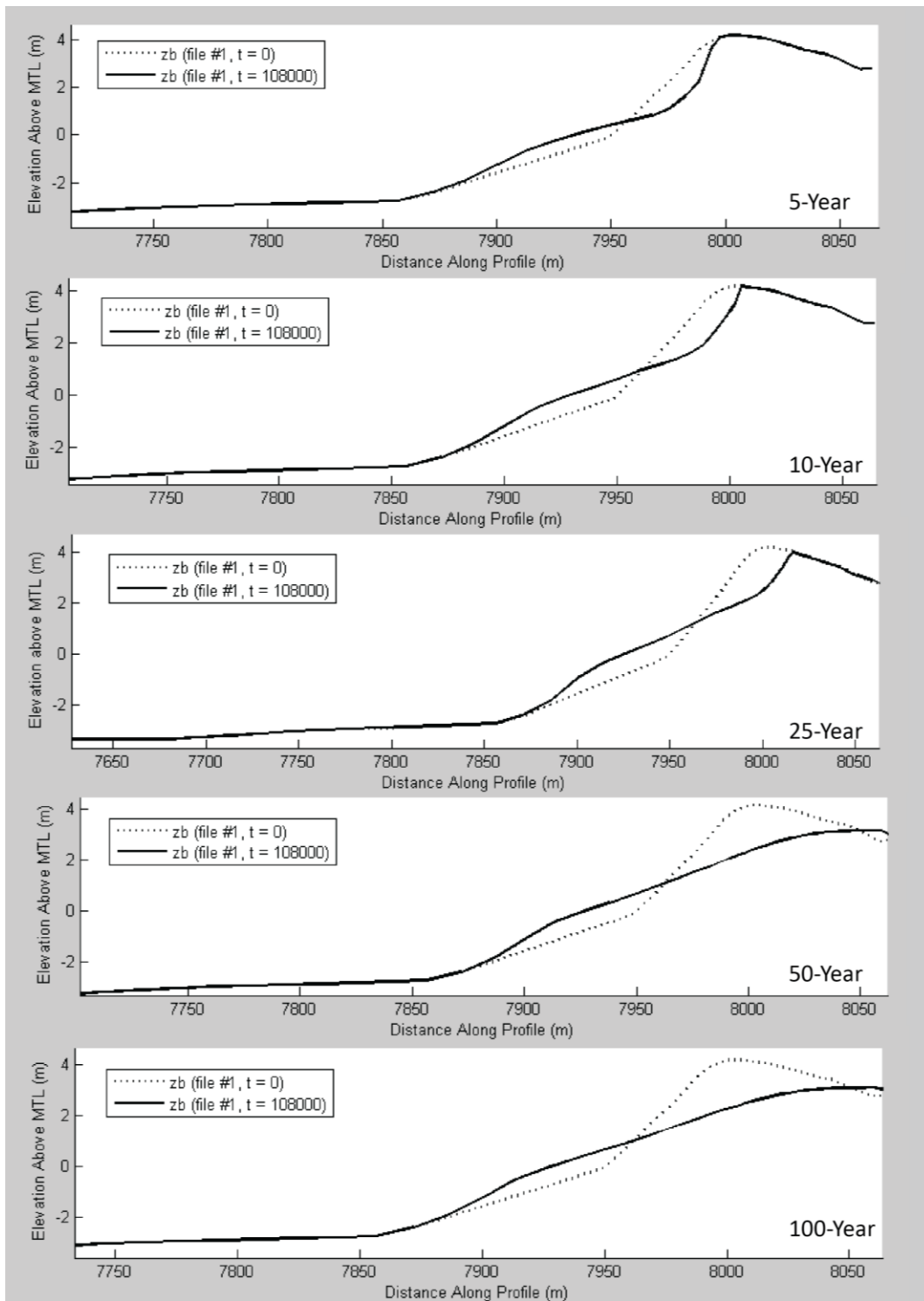


Figure 4.10—Profile 3 morphological changes with varying storm frequency of 5, 10, 25, 50, and 100 years, from time 0 to time of 108000 seconds.

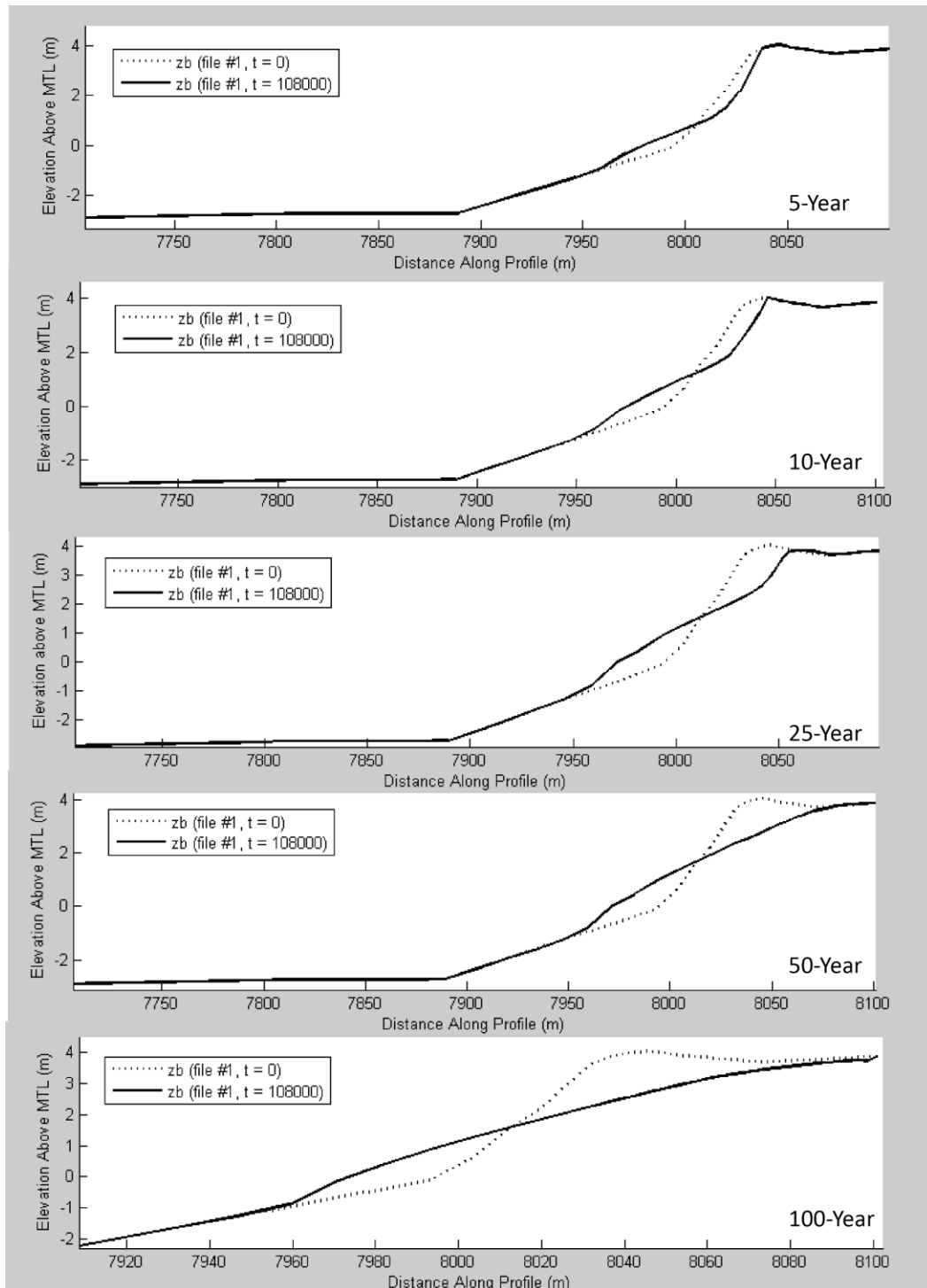


Figure 4.11—Profile 4 morphological changes with varying storm frequency of 5, 10, 25, 50, and 100 years, from time 0 to time of 108000 seconds.



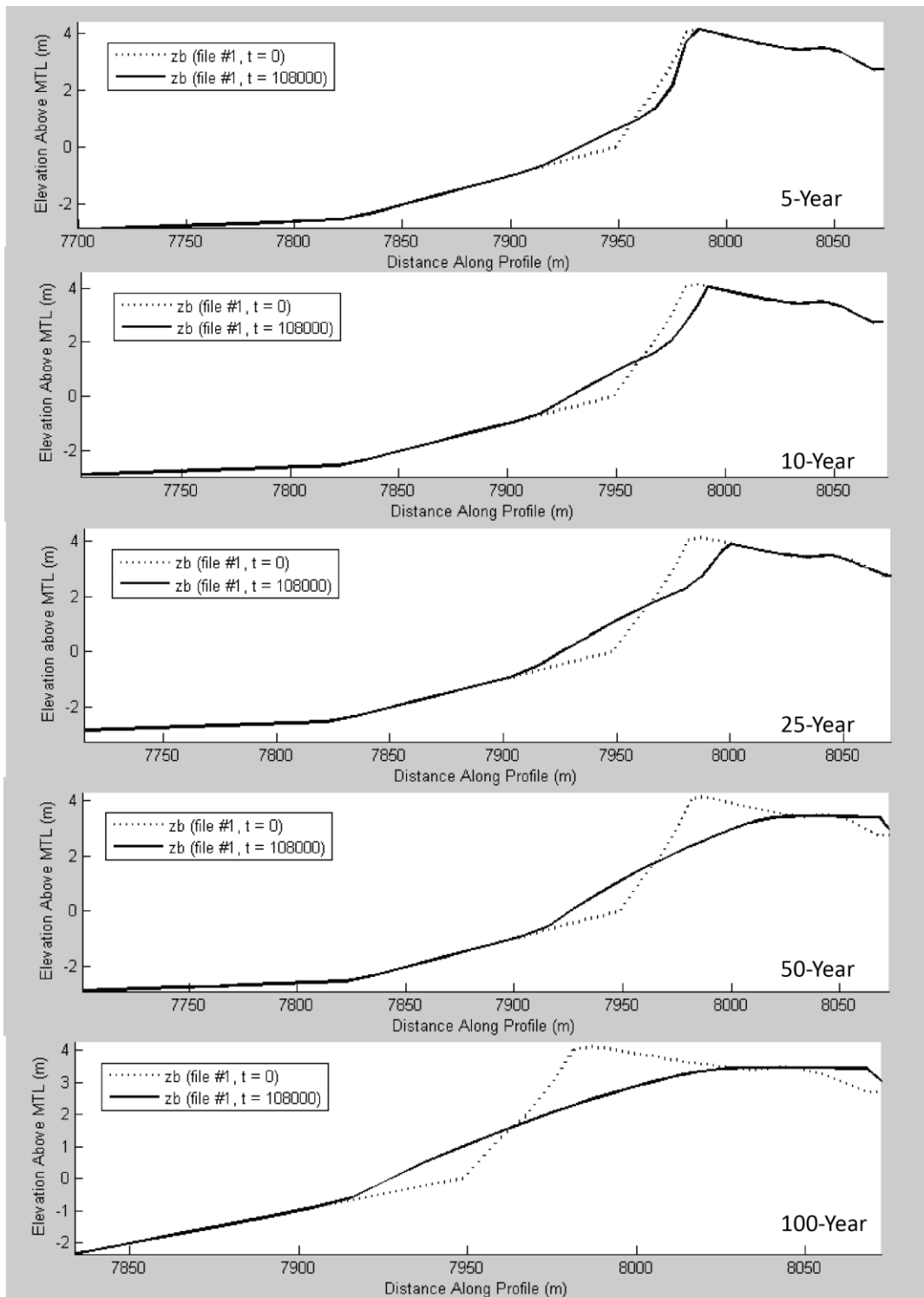


Figure 4.12—Profile 5 morphological changes with varying storm frequency of 5, 10, 25, 50, and 100 years, from time 0 to time of 108000 seconds, zoomed-in on 100-year storm results.

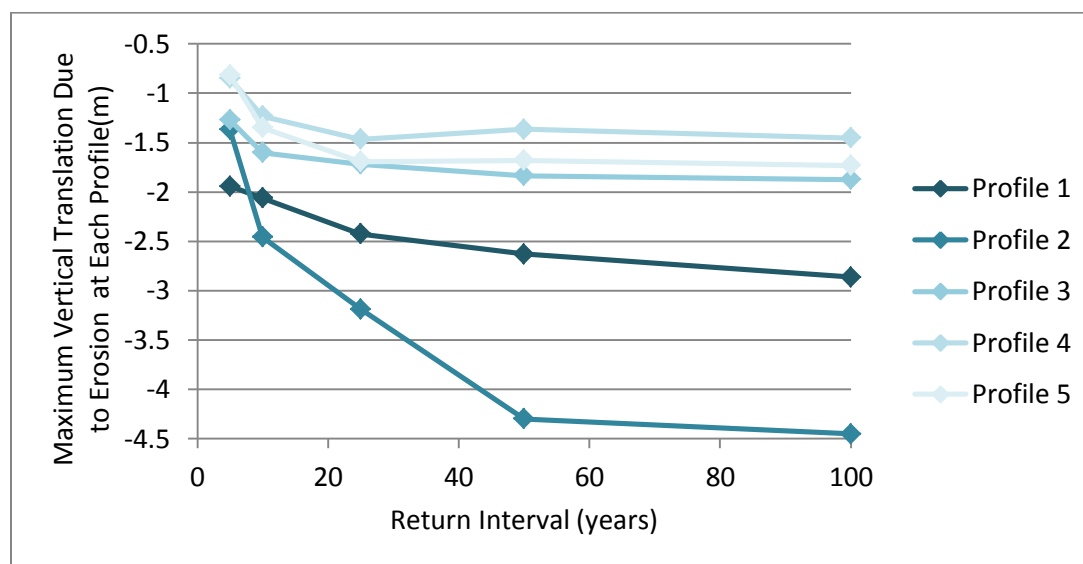


Figure 4.13—Maximum vertical translation due to erosion at each profile.

The modeled values for vertical translation of sediments (Figure 4.13) may have been exaggerated because of the potential effects of snow and ice. The calibration storm occurred during a time-period when no sea ice or snow was present on the beach face. This, however, is not always the case, and is more likely to not be the case for large storm late in the. For example, the storm measured by the Alaska DGGS in November 2011 was much larger than the calibration storm, and occurred during frozen beach conditions with ice slush in the water that was transported onshore (Figure 4.14). Frozen sea and beach conditions would likely change the spit's morphological response to storm events, however, the data used to validate the storm were taken from unfrozen conditions. Frozen beach conditions would likely reduce erosivity of the beach face during storm events, because of the ability of the ice to increase material strength. Moreover, a smoother beach surface would reduce friction in the swash zone, which

may increase runup. These factors would result in increased maximum water elevations and reduced erosion on the frozen beach. Slush in the water would dampen, or limit, the generation of wind-driven waves, reducing their effect on increased water elevations and wave attack at the coastline. Without a better understanding of these mechanics, the conditions were assumed to be similar to unfrozen conditions.



Figure 4.14—Frozen slush deposited by November 2011 Bering Sea Storm.

The maximum water elevations were mapped onto a digital elevation model created by the Alaska Department of Commerce, Community, and Economic Development (DCCED) (Figure 4.15). The map depicts the maximum extent of flooding on both sides of the lagoon at the return intervals modeled in this analysis (5-100-years). Potential erosion was not mapped relative to the storm events, because of the likelihood of beach recovery after each storm. The map also includes, for comparative purposes, runup elevations measured by the Alaska DGGS

from the November 2011. The locations of the runup elevations around the spit were most similar to the 10-year flooding return interval. There may be a discrepancy between the mapped inundation extents, and actual extents because of the increase in road elevation near the fuel storage facilities (Figure 4.15). The digital elevation model used in this study was made before the increase in road elevation, which reduced the flooding on that surface.



Figure 4.15—Flooding projections on the Golovin spit from numerical modeling and measured storm events, projected in NAD83 State Plane, Alaska 7 (in feet), datum NGVD 27 (feet). Base map is an aerial photograph flown in June 2004, provided by the Alaska DCCED (all elevations and spatial references were provided in feet for the use of these values by the community of Golovin in the future).

A storm occurred in 1992 that was mapped on the Alaska DCCED Golovin community map (DCCED, 2004). Although the flooding that occurred in 1992 was before changes in road elevations were made, the event was most similar to a 10-25 year storm. Both measured storms were at least 10-year return interval storms and measured within the last 20 years. Other storms that may have occurred during this time period were not measured. Anecdotally, no contemporary oral records indicate storms reaching elevations that could have induced overwash of the entire spit in the past 100 years.

The values for runup calculated from the 50 and 100-year return intervals were highly dependent on modeled outputs from the USACE. Predictions were made using 16 years of water level data available at the Nome tide station (Chapman et al., 2009). Since the water level record did not extend to the highest return interval frequency analyzed here, some error may have been propagated into the hind-casted extrapolation of the 50-100-year storms, resulting in overestimation of maximum runup elevations. The results of the modeling completed in this study were similar to values modeled for Shaktoolik, Alaska, using similar global model inputs (USACE, 2011b). Complete overwash of the Shaktoolik spit was also expected at the 50-year return interval (USACE, 2011b).

After the field excursion in October 2013, a storm event reaching 3.14 m above MTL was expected at Golovin. We were, however, unable to measure shoreline change or maximum water elevations after this event because of limited project funds. Members of the community of Golovin did construct a temporary levee on the lagoon side of the spit in preparation for this storm (Figure 4.16), which helped to remediate flooding in the community.

Temporary berms are good options for remediation of coastal flooding. These structures are constructed at many locations along the California coast (Sanders, Schubert, Gallien, &



Shakeri Majd, 2013) during higher energy periods such as winter. They have been found to reduce the amount of flooding during storm events, even if the berm is damaged during the event, with total berm failure occurring when the swash reaches 25-30% of total berm height (Sanders et al., 2013). If communities are able to construct these features during storm seasons, they may have less impact on the economic use of beaches during other times of the year. For Golovin, temporary berms may reduce flooding on the bay side of the spit, however, since flooding occurs on such a regular interval, a more permanent structure should be built on the lagoon side of the spit, where there is maximum flooding vulnerability. Currently, available real-time models give four days advance prediction of storm water elevations, which may be enough time for a well-organized community to establish a temporary berm on a storm-by-storm basis. For small populations, such as in Golovin, however, finding the resources to construct a temporary berm each year may be challenging.



Figure 4.16—Temporary levee constructed before November 2013 storm, photo by Carol Oliver.

Since 10-25-year storms have been documented at Golovin within the last 20 years, the corresponding runup elevations should be used for the minimum design storm height considered for engineered structures on the spit. Storm events above the 25-year return interval were found to induce overwash of the entire spit. If this occurred, there would be little that could be done, from an engineering perspective, to prevent inundation of community infrastructure. However, plans may be made for evacuation of residents from the low-lying elevations to a community shelter during storms of these magnitudes. These evacuation plans should be practiced ahead of time, to increase storm preparedness.

#### 4.5 Conclusions

This work provides an estimate of flooding and sediment redistribution as a result of storm surge on the Golovin spit using XBeach numerical modeling. The modeled morphological responses to the storm events include vertical translation of sediment (erosion) at or near the vegetation line and reductions in beach slope, however, these changes aren't expected to be sustained over time since the sediments were redistributed to a nearshore bar. This mechanism is supported by historical shoreline positions, which have been shown to be dynamically stable since 1972. Shoreline stabilization is not recommended as a high priority engineering project for Golovin.

The maximum water elevations reached on the spit were projected to occur on the lagoon side, at about 1.08 times the magnitude of runup on the bay side of the spit. These values were used to map the potential inundation around the spit for differing return intervals of storm elevations. Measured storm elevations reached the 10-25-year return interval during storms in 2011 and 1992. However, measurements were not made after other storm events in the region.

Maximum water elevations (runup) on the Golovin coast should be considered for engineering design of a permanent remediation structure, such as a levee on the lagoon side of the spit, or for a temporary berm on bay side of the spit. Either of these options may help to reduce flooding in the low-lying parts of the community due to storm surge at the 25-year return interval. The values modeled for maximum water elevation may be subject to error from long-term hindcasting extrapolation, and should be updated as global model inputs are enhanced, and more oceanographic data becomes available for the region.





## **5.0 Conclusions and Future Work**

**1. Golovin is not subject to contemporary and sustained erosional trends on the spit coastline. Storm surges may, however, contribute to episodic erosion of the beach, which is replenished over time.**

The community of Golovin, Alaska, is subject to episodic flooding and erosion from the inundation of storm surges entering Norton Sound. Although sediments are transported during these events, the long-term effects are minimal. Neither erosion nor accretion dominates the spit environment. This was observed in the aerial photography and satellite imagery dating from 1972 to 2013. The results of the numerical models also showed transport of sediments to the nearshore zone during storms of 5-100-year return intervals, which is indicative of sediment retention. Some locations around the spit experience more dynamic shoreline positions, these regions, however, are located farther from infrastructure than locations with less dynamic shoreline positions.

**2. Remote sensing methods can enhance oceanographic datasets in northwest Alaska.**

Depths extracted from WorldView-2 satellite imagery were found to be a useful dataset to augment and improve the continuity and spatial resolution of bathymetric data around the Golovin spit. Although depths were not derived for locations affected by suspended sediment, and the measured depth to predicted depth relationship began to deteriorate at depths below 3.88 m (+/-0.43 m), the predicted values were still valuable as inputs for numerical modeling purposes. In the future, new image collections for this type of analysis should be procured during the highest influx of solar radiation (summer), and at locations where suspended sediment is correlated to bottom topography. The Landsat-8 satellite has the potential to

provide similar data as the WorldView-2 satellite spectrally, and should be considered for future studies.

**3. Storm surge-induced flooding is expected to inundate coastal infrastructure in the next 25-100 years based on the results of updated numerical modeling.**

The 5-year storm event is expected to extend adjacent to most buildings on the Golovin spit, while the 25-year storm is expected to inundate most coastal infrastructure beginning on the lagoon side, barring new engineering solutions. Historically, measured storm events agree with these results, however, changes to road elevations and temporary placement of berms may reduce the extent of flooding from the lagoon side.

Overwash of the entire spit is expected to occur at the 50-100-year return interval. Although there is no contemporary oral record of complete overwash of the spit, the results are similar to other modeling efforts in Norton Sound (Shaktoolik). If the values projected here are overestimations, we must consider updating and refining the global model inputs (WAM Cycle 4.5 and ADCIRC). Any data described for this region is subject to the lack of recording systems for wave and water level data and regional scale availability, which should be enhanced in the future.

**4. In-depth, community-based analysis of coastal hazards can contribute to enhanced engineering design beyond anecdotal perception of such hazards.**

Despite perceptions by the public, media, and generalized documentation, Golovin may be less at risk to erosion than is reported. There is, however, regular flooding that occurs on a 5-10 year interval, with increased frequency during positive phase AO cycles. These discrepancies

in perception may lead to overestimations in engineering design, but the results of this study should be considered before the community decides to build a permanent or temporary remediation structure. This may be the case for many other communities in Northwest Alaska facing similar geohazards as Golovin. Although in-depth analysis on a community-by-community basis is expensive, these analyses may save money by applying site-specific engineering designs to remedy such hazards. This form of analysis, if performed at all sites subject to hazardous conditions, would also give coastal managers and planners a prioritization system as to which hazards should be addressed immediately, and which hazards may be addressed over time, allocating state and federal funding based on community needs.



## References

- ACCAP, & SNAP. (2014). Historical sea ice concentration. Retrieved 02/20/2014, from Alaska Center for Climate Assessment and Policy and Scenarios Network for Alaska and Arctic Planning <http://seaiceatlas.snap.uaf.edu/explore#location/1850/01/67.00/-162.25/71>
- Alaska, State of. (2008). Recommendations report to the Governor's Subcabinet on Climate Change: State of Alaska.
- Alaska, State of. (2009). Recommendations to the Governor's Subcabinet on Climate Change: State of Alaska.
- Alaska, State of. (2010). Golovin, 2010 Population and Housing Characteristics. Retrieved 01/04/2014 <http://commerce.alaska.gov/cra/DCRAExternal/Community/Details/b45416b3-6619-4f0a-9a0b-7e236e56992a>
- Blier, Warren, Keefe, Stanley, Shaffer, Wilson A., & Kim, Sung C. (1997). Storm surges in the region of western Alaska. *Monthly Weather Review*, 125, 3094-3108.
- Buscombe, D., Rubin, D.M., & Warrick, J.A. (2010). A universal approximation of grain size from images of noncohesive sediment. *Journal of Geophysical Research*, 115, 17.
- Chapman, Raymond, S., Kim, Sung-Chan, & Mark, D.J. (2009). Storm-induced water level prediction study for the western coast of Alaska: U.S. Army Corps of Engineers, Coastal and Hydraulics Laboratory.
- DCCED. (2004). Community Map Golovin: Alaska Department of Commerce, Community, and Economic Development
- DCCED. (2014). Quarterly Report: 2014, October-December (Q2) Golovin. Retrieved 01/04/2014, from State of Alaska Department of Commerce, Community, and Economic

Development

<http://commerce.alaska.gov/cra/DCRAExternal/RUBA/ViewReport/43da147d-dc66-4481-9306-4223c773436f>

Del Rio, Laura, & Garcia, Javier F. (2014). Error determination in the photogrammetric assessment of shoreline changes.

[http://rodin.uca.es/xmlui/bitstream/handle/10498/15668/NatHaz2013\\_DelRio%20and%20Gracia\\_manuscriptaccepted.pdf?sequence=2](http://rodin.uca.es/xmlui/bitstream/handle/10498/15668/NatHaz2013_DelRio%20and%20Gracia_manuscriptaccepted.pdf?sequence=2)

Diedda, M., & Sanna, G. (2012). Bathymetric Extraction Using Worldview-2 High Resolution Images. *International Archives of the Photogrammetry, Remote Sensing and Spatial Information Sciences, XXXIX-B8*.

Douglas, D.C. (2010). Arctic sea ice decline-Projected changes in timing and extent of sea ice in the Bering and Chuckchi Seas: U.S. Geological Survey Open File-Report 2010-1176.

Globe, Digital. (2011). Bathymetry Data Sheet. 2.

ISUST. (2013). ASOS/AWOS data download.

[http://mesonet.agron.iastate.edu/request/download.phtml?network=AK\\_ASOS](http://mesonet.agron.iastate.edu/request/download.phtml?network=AK_ASOS)

Johnson, Walter R., & Kowalik, Zygmunt. (1986). Modeling of storm surges in the Bering Sea and Norton Sound. *Journal of Geophysical Research, 91*, 5119-5128.

Kanno, Ariyo, & Tanaka, Yoji. (2012). Modified Lyzenga's Method for Estimating Generalized Coefficients of Satellite-Based Predictor of Shallow Water Depth. *IEEE Geoscience and Remote Sensing Letters, 9(4)*, 715-719.

Kinsman, N.E.M., & DeRaps, M.R. (2012). Coastal hazard field activities in response to the November 2011 Bering Sea storm, Norton Sound, Alaska: Alaska Division of Geological & Geophysical Surveys Report of Investigation.

Komar, Paul D. (1998). *Beach Processes and Sedimentation*. Upper Saddle River, NJ: Pearson Education.

Lee, Krista R., Olson, Richard C., & Kruse, Fred A. (2012). *Using multi-angle WorldView-2 imagery to determine ocean depth near the island of Oahu, Hawaii*. Paper presented at the Algorithms and Technologies for Multispectral, Hyperspectral, and Ultraspectral Imagery XVIII.

Lyzenga, D.R. (1978). Passive remote sensing techniques for mapping water depth and bottom features. *Applied Optics*, 17.

Lyzenga, D.R. (1985). Shallow-water bathymetry using combined lidar and passive multispectral scanner data. *International Journal of Remote Sensing*, 6, 115-125.

Madden, C.K. (2009). *Contributions to Remote Sensing of Shallow Water Depth with the WorldView-2 Yellow Band*. (Master of Science), Naval Postgraduate School, Monterey, California.

Mason, Owen K., Jordan, James W., Lestak, Leanne, & Manley, William F. (2012). Narratives of Shoreline Erosion and Protection at Shishmaref, Alaska: The Anecdotal and the Analytical. *Pitfalls of Shoreline Stabilization*, 3, 73-92.

Miecznik, Gregorz, & Grabowska, Dorota. (2012). *WorldView-2 bathymetric capabilities*. Paper presented at the Algorithms and Technologies for Multispectral, Hyperspectral, and Ultraspectral Imagery XVIII.

Mikulski, Pearl. (2009). Golovin Local Economic Development Plan 2009-2013: Kawerak, Inc.

Moore, Laura J., Ruggiero, Peter, & List, Jefferey H. (2006). Comparing Mean High Water and High Water Line Shorelines: Should Proxy-Datum Offsets be Incorporated into Shoreline Change Analysis? *Journal of Coastal Research*, 22(4), 894-905.



- NOAA. (1900). Hydrographic Sheet No. 2482: Golovnin Lagoon. Retrieved 03/23/2014, from National Oceanic and Atmospheric Administration National Geophysical Data Center [http://www.ngdc.noaa.gov/nndc/struts/results?op\\_0=eq&t=103118&s=2&d=3&d=4&d=18&d=6&d=20&d=25&d=22&d=23&d=24&d=19&d=7&d=5&d=21&d=8&d=9&d=10&d=11&d=12&d=13&d=14&d=16&d=17&d=15&no\\_data=suppress&v\\_0=H02482](http://www.ngdc.noaa.gov/nndc/struts/results?op_0=eq&t=103118&s=2&d=3&d=4&d=18&d=6&d=20&d=25&d=22&d=23&d=24&d=19&d=7&d=5&d=21&d=8&d=9&d=10&d=11&d=12&d=13&d=14&d=16&d=17&d=15&no_data=suppress&v_0=H02482)
- NOAA. (2013). Tides and Currents. Retrieved 01/04/2014, from National Oceanic and Atmospheric Administration <http://tidesandcurrents.noaa.gov/tides10/tab2wc2c.html>
- NOAA. (2014a). National Weather Service, Climate Prediction Center, Climate Glossary: National Oceanic and Atmospheric Administration.
- NOAA. (2014b). Understanding Coastal Inundation. Retrieved 03/23/2014, from National Oceanic and Atmospheric Administration <https://www.csc.noaa.gov/digitalcoast/inundation/understand>
- OCSEAP. (1984). The Norton Basin Environment and Possible Consequences of Planned Offshore Oil and Gas Development (pp. 119). Anchorage, AK: Outer Continental Shelf Environmental Assessment Program.
- Ostrom, J.E., Comiskey, A.L., & Miller, R.C. (1986). Atlas of Oceanographic Information for Norton Sound, Alaska. New London, CT: U.S. Coast Guard Academy.
- Pawlowicz, Rich, Beardsley, Bob, & Lentz, Steve. (2002). Classical tidal harmonic analysis including error estimates in MATLAB using T\_TIDE. *Computers & Geosciences*, 28, 9.
- Robertson, William V., Whitman, Dean, Zhang, Keqi, & Leatherman, Stephen P. (2004). Mapping Shoreline Position Using Airborne Laser Altimetry. *Journal of Coastal Research*, 20(3), 884-892.

- Roelvink, Dano, Reniers, Ad, Dongeren, Ap van, Thiel de Vries, Jaap van, Lescinski, Jamie, & McCall, Robert. (2010). XBeach Model Description and Manual (6 ed.): Unesco-IHE Institute for Water Education, Deltares and Delft University of Technology.
- Roelvink, Dano, Reniers, Ad, Dongeren, Ap van, Thiel de Vries, Jaap van, McCall, Robert, & Lescinski, Jamie. (2009). Modelling storm impacts on beaches, dunes and barrier islands. *Coastal Engineering*, 56, 1133-1152.
- Sagawa, Tatsuyuki, Boisnier, Etienne, Komatsu, Teruhisa, Mustapha, Karim Ben, Hattour, Abdalla, Kosaka, Naoko, & Miyazaki, Sanae. (2010). Using bottom surface reflectance to map coastal marine areas: a new application method for Lyzenga's model. *International Journal of Remote Sensing*, 31(12), 3051-3064.
- Sallenger, Asbury H., Jr. (1983). Measurements of debris-line elevations and beach profiles following a major storm: Northern Bering Sea coast of Alaska. Menlo Park, CA: U.S. Geological Survey Open-File Report 83-394.
- Sallenger, Asbury H., Jr. (2000). Storm Impact Scale for Barrier Islands. *Journal of Coastal Research*, 16(3), 890-895.
- Sanders, B.F., Schubert, J.E., Gallien, T., & Shakeri Majd, M. (2013). *Terrestrial laser scanning of anthropogenic beach berms for urban flood defense*. Paper presented at the 2013 Fall Meeting AGU, San Francisco, CA.
- Smith, Jacquelyn R., Kinsman, N.E.M., & Misra, Debasmita. (2013). Using Worldview-2 multispectral bands for shallow water bathymetric survey near Wales, Alaska (pp. 1). Alaska Division of Geological & Geophysical Surveys: American Society of Photogrammetry and Remote Sensing Annual Meeting.

- Thieler, E.R., Himmelstoss, E.A., Zichichi, J.L., & Erugl, Ayhan. (2009). Digital Shoreline Analysis System (DSAS) version 4.0- An ArcGIS extension for calculating shoreline change: U.S. Geological Survey.
- Till, A.B., Dumoulin, J.A., Weldon, M.B., & Bleick, H.A. (2010). Preliminary Bedrock Geologic Map of the Seward Peninsula, Alaska.
- Trantino, Cristina, Adamo, Maria, Pasquariello, Guido, Lovergine, Francesco, Blonda, Palma, & Tomaselli, Valeria. (2012). 8-Band Image Data Processing of the Worldview-2 Satellite in a Wide Area of Applications. *Earth Observation*, 973-978.
- USACE. (2009). Alaska baseline erosion assessment, study findings and technical report. Elmendorf Airforce Base, AK: U.S. Army Corps of Engineers.
- USACE. (2011a). Golovin Flood Hazard Data (pp. 1): U.S. Army Corps of Engineers.
- USACE. (2011b). Shaktoolik Coastal Flooding Analysis (pp. 18): U.S. Army Corps of Engineers Coastal and Hydraulics Laboratory, Denali Commission.
- USACE. (2013). *Wave Information Studies*. U.S. Army Corps of Engineers. Retrieved from <http://wis.usace.army.mil/hindcasts.shtml?dmn=alaskaWIS>
- USGAO. (2003). Alaska Native Villages: Most are Affected by Flooding and Erosion, but Few Qualify for Federal Assistance: U.S. General Accounting Office.
- USGAO. (2009). Report to congressional requestors-Alaska Native villages, limited progress has been made on relocating villages impacted by flooding and erosion: U.S. Government Accountability Office.
- USGS. (2013). Coastal Hazards: Hurricanes and Extreme Storms. Retrieved 03/22/2014, from U.S. Geological Survey <http://coastal.er.usgs.gov/hurricanes/impact-scale/inundation.php>

- Vousdoukas, M.I., Almeida, L.P., & Ferreira, O. (2011). Modelling storm-induced beach morphological change in a meso-tidal, reflective beach using XBeach. *Journal of Coastal Research*(Special Issue (64)), 1916-1920.
- Warrick, Jonathan A., Rubin, David M., Ruggiero, Peter, Harney, Jodi N., Draut, Amy E., & Buscombe, Daniel. (2009). Cobble cam: grain-size measurements of sand to boulder from digital photographs and autocorrelation analyses. *Earth Surface Processes and Landforms*, 34, 1811-1821.
- Wise, James L., Comiskey, Albert L., & Becker, Richard Jr. (1981). Storm surge climatology and forecasting in Alaska. Anchorage, AK: Arctic Environmental Information and Data Center University of Alaska.